Sox17 Regulates a Program of Oligodendrocyte Progenitor Cell Expansion and Differentiation during Development and Repair

Li-Jin Chew, Xiaotian Ming, Brian Mcellin, Jeffrey Dupree, Elim Hong, Mackenzie Catron, Melissa Fauveau, Brahim Nait-Oumesmar, Vittorio Gallo

Article

Cell Reports

Sox17 Regulates a Program of Oligodendrocyte Progenitor Cell Expansion and Differentiation during Development and Repair

Graphical Abstract

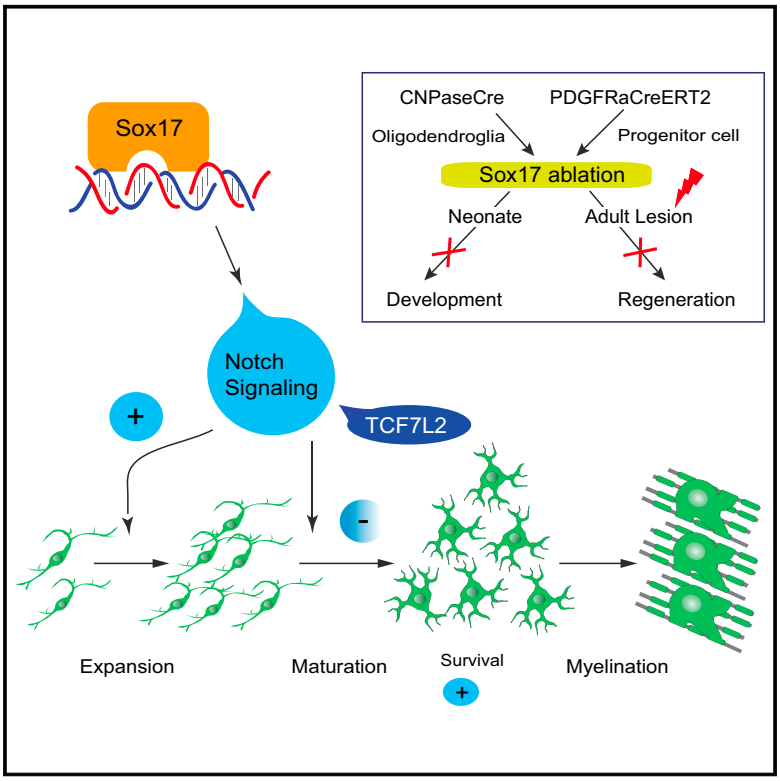

Highlights

- Sox17 ablation in CNS *in vivo* impairs oligodendrocyte development and regeneration
- Sox17 promotes both oligodendrocyte progenitor expansion and maturation *in vivo*
- Notch signaling mediates oligodendrocyte progenitor cell maintenance by Sox17
- TCF7L2 expression in oligodendrocytes is regulated by Sox17 and Notch signaling

Authors

Li-Jin Chew, Xiaotian Ming, Brian McEllin, ..., Melissa Fauveau, Brahim Nait-Oumesmar, Vittorio Gallo

Correspondence

lchew@childrensnational.org (L.-J.C.), vgallo@childrensnational.org (V.G.)

In Brief

Oligodendrocyte development is controlled by sequential processes of progenitor cell proliferation and differentiation, believed to be largely regulated by distinct mechanisms. Chew et al. characterize white matter abnormalities in brains of Sox17-deficient mice and identify the candidate Sox17-regulated target genes Notch and TCF7L2, which mediate progenitor cell expansion and maturation, respectively.

Chew et al., 2019, Cell Reports *29*, 3173–3186
December 3, 2019
https://doi.org/10.1016/j.celrep.2019.10.121

CellPress

Cell Reports
Article

Sox17 Regulates a Program of Oligodendrocyte Progenitor Cell Expansion and Differentiation during Development and Repair

Li-Jin Chew,[1,*] Xiaotian Ming,[1] Brian McEllin,[1] Jeffrey Dupree,[2,3] Elim Hong,[1] Mackenzie Catron,[1] Melissa Fauveau,[4] Brahim Nait-Oumesmar,[4] and Vittorio Gallo[1,5,*]
[1]Center for Neuroscience Research, Children's National Hospital, Washington, DC 20010, USA
[2]Department of Anatomy and Neurobiology, Virginia Commonwealth University Medical Center, Richmond, VA, USA
[3]Research Service, Hunter Holmes McGuire VA Medical Center, Richmond, VA 23249, USA
[4]Institut du Cerveau et de la Moelle Épinière, ICM, INSERM U1127, CNRS UMR7225, Sorbonne Université, Hôpital de la Pitié-Salpêtrière, 75013 Paris, France
[5]Lead Contact
*Correspondence: lchew@childrensnational.org (L.-J.C.), vgallo@childrensnational.org (V.G.)
https://doi.org/10.1016/j.celrep.2019.10.121

SUMMARY

Sox17, a SoxF family member transiently upregulated during postnatal oligodendrocyte (OL) development, promotes OL cell differentiation, but its function in white matter development and pathology *in vivo* is unknown. Our analysis of oligodendroglial- and OL-progenitor-cell-targeted ablation *in vivo* using a floxed Sox17 mouse establishes a dependence of postnatal oligodendrogenesis on Sox17 and reveals Notch signaling as a mediator of Sox17 function. Following Sox17 ablation, reduced numbers of Olig2-expressing cells and mature OLs led to developmental hypomyelination and motor dysfunction. After demyelination, Sox17 deficiency inhibited OL regeneration. OL decline was unexpectedly preceded by transiently increased differentiation and a reduction of OL progenitor cells. Evidence of a dual role for Sox17 in progenitor cell expansion by Notch and differentiation involving TCF7L2 expression were found. A program of progenitor expansion and differentiation promoted by Sox17 through Notch thus contributes to OL production and determines the outcome of white matter repair.

INTRODUCTION

SRY-Box (Sox)-containing transcription factors are evolutionarily conserved proteins (Gubbay et al., 1990) that are essential for the differentiation and maturation of a variety of tissue systems, including the developing nervous system (Chew and Gallo, 2009; Stolt and Wegner, 2010). Unlike the Sox D and E families, studies showing the physiological role of Sox F family members in the CNS *in vivo* are lacking, and Sox17 remains as the only member of the Sox F with established involvement in CNS glia development (Sohn et al., 2006). Sox17 was originally identified as an obligate endodermal determinant (Kanai-Azuma et al., 2002), whereas Sox7, 17, and 18 regulate the vasculature (Matsui et al., 2006; Wat and Wat, 2014). In the postnatal mouse white matter (WM), Sox17 expression is developmentally associated with that of multiple myelin genes, and its peak of expression in pre-myelinating oligodendrocytes (OLs) is consistent with a role in regulating the transition to immature OLs (Sohn et al., 2006). In the OL lineage, Sox17 regulates the Wingless/Int-1 (Wnt)/beta catenin signaling pathway and progenitor cell differentiation (Chew et al., 2011). Consistent with a role in OL regeneration, recent studies have shown that Sox17 expression in multiple sclerosis and experimental demyelinated lesions is localized in newly generated OL cells of actively remyelinating WM (Moll et al., 2013). However, functional involvement of endogenous Sox17 in postnatal OL development and regeneration in WM *in vivo* has not been investigated.

We have generated a conditional mouse allele to study Sox17 function in the oligodendroglia lineage *in vivo* by breeding this floxed strain with the CNP-Cre strain (Lappe-Siefke et al., 2003). Our characterization shows that Sox17 ablation disrupts OL differentiation in the postnatal subcortical WM. In contrast to previous *in vitro* studies of Sox17, the evidence indicates that OL loss arises initially from a reduction in oligodendrocyte progenitor cells (OPCs). The eventual decrease in OL lineage cells was accompanied by reduced myelin protein expression, thin myelin sheaths, and motor deficits. Sox17 ablation using *PDGFRα*CreER^{T2} produced similar changes in progenitor cells and OLs, indicating a progenitor-specific role for Sox17. In addition, Sox17 ablation resulted in a significantly reduced capacity for OL regeneration following lyso-phosphatidylcholine (LPC)-induced demyelination. Similar to postnatal development, OPC induction was reduced and fewer mature OLs were observed in Sox17-deficient WM lesions. In addition to Sox17 regulation of Notch1 receptor and Hes effectors, we identified TCF7L2 expression to be regulated by both Sox17 and Notch. These studies demonstrate that Sox17 plays an important role in promoting a program of OL development by progenitor expansion and maturation and which operates to regulate the regenerative potential of the adult WM.

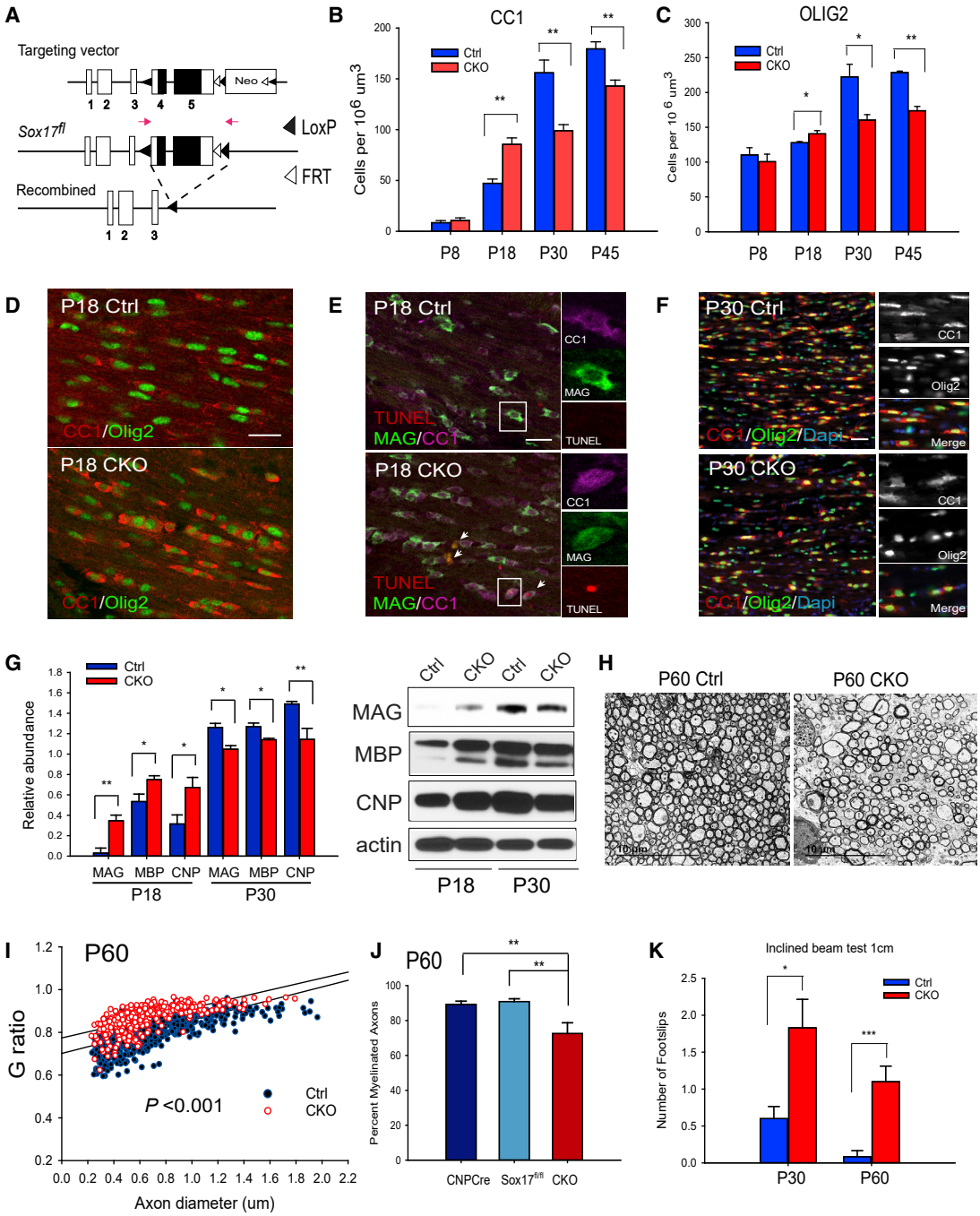

Figure 1. Targeted Sox17 Ablation Impairs Oligodendrocyte Development and Myelination

(A) Sox17 conditional allele with LoxP sites (black triangles) flanking exons 4 and 5. CNP-Cre-mediated excision produces the recombined allele lacking the protein-coding region (black boxes). See also Figure S1.

(B–D) Immunohistochemical analysis of postnatal oligodendrocyte (OL) development, with quantification of CC1 (B) and Olig2 (C) cells. Note increased CC1 and Olig2 cells at P18 (D). n = 3–6. *p < 0.05 and **p < 0.01, Student's unpaired t test, mean ± SEM.

(E) TUNEL analysis in P18 CKO shows colocalized TUNEL (red) with CC1 (magenta) and MAG (green).

(F) Decreased OLs CC1 (red) and Olig2 (green) in P30 CKO indicates OL deficit. Color information was removed for CC1 and Olig2 insets.

(G) Western blotting indicates biphasic change in myelin proteins between P18 and P30. n = 3. *p < 0.05 and **p < 0.01, Student's unpaired t test, mean ± SEM.

(H) Transmission electron microscopy indicates hypomyelination in P60 CKO. n = 3–11.

(I) G-ratio analysis shows significantly increased values for CKO at P60 arising from thinner myelin, as the average diameter of myelinated axons remained unchanged.

(legend continued on next page)

RESULTS

Targeted Ablation of Sox17 in the Oligodendroglial Lineage Decreases Sox17 Expression

To determine the physiological role of Sox17 in developing OLs, a conditional mouse Sox17 allele was created. This Sox17 allele has exons 4 and 5 flanked by loxP sites, allowing for Cre-mediated excision of the two largest exons (Figure 1A). Genomic deletion of Sox17 exons 4 and 5 that was validated by PCR was performed on DNA isolated from subcortical white matter (SCWM) of CNP-Cre$^{/+}$;Sox17$^{f/f}$ (conditional knockout [CKO]) and Cre-negative (control [Ctrl]) littermates (Figure S1A). Decreased Sox17 expression *in vivo* was previously shown in fluorescence-activated cell sorting (FACS)-purified OL lineage cells of this conditional mutant at postnatal day 10 (P10) (Chew et al., 2011). Quantitative PCR using P18 WM tissue showed reduced Sox17 and myelin protein RNA (Figure S1B).

Sox17 Ablation Decreases the Number of WM OLs

Previous characterization of Sox17 expression in WM OLs, as well as loss- and gain-of-function studies in cultured OPCs indicate a role for Sox17 in OL development (Sohn et al., 2006). We, therefore, hypothesized that Sox17 ablation in the OL lineage would impair progenitor cell differentiation and lead to a reduction of mature OLs, with functional deficits resulting from developmental hypomyelination. Immunohistochemical characterization of subcortical WM in either CNP-Cre/$^{+}$;Sox17$^{+/+}$ (CNP-Cre), or Cre-negative (Ctrl) and CKO mice over the course of postnatal development revealed age-specific changes in the numbers of oligodendroglial lineage cells. Myelinating OLs labeled with the mouse monoclonal antibody clone CC1 were significantly reduced in the Sox17 CKO animals at P30 and P45 (Figure 1B). A reduction in mature MAG^{+} OLs was observed at P30 and P45 (Figure S1C). The number Olig2 cells was also decreased at P30 and P45 (Figure 1C). Interestingly, there was a significant increase in OLs at P18 (Figures 1B–1D). This transient rise in differentiation was accompanied by reduced cell survival, as total terminal deoxynucleotidyl transferase dUTP nick end labeling (TUNEL) staining showed a modest but significant increase in CKO WM (1.6714 ± 0.922 versus 5.987 ± 1.065 per 10^6 μm^3, p = 0.01085 Student's unpaired t test). TUNEL^{+} cells included CC1^{+} and MAG^{+} OLs (Figure 1E), likely contributing to OL loss by P30 (Figure 1F). The protein levels of myelin proteins were also analyzed across development by using micro-dissected corpus callosum from *CKO* and wild-type (WT) siblings. Accordingly, a transient increase in MBP, CNP, MAG protein levels at P18 in *Sox17* mutants was followed by a significant decrease in these proteins at P30 compared with littermate controls (Figure 1G).

Sox17 Ablation Causes Myelin Thinning and Impairs Motor Coordination

To determine whether the decline in OLs affected myelination, we analyzed axonal ultrastructure by transmission electron microscopy. Figure 1H shows that, although the average diameter of myelinated axons and axonal integrity remained unchanged, myelin thickness, as quantified in Figure 1I by G ratio, was significantly reduced, together with a decrease in myelinated axons (Figure 1J). The size of the corpus callosum was also found to be reduced in P30 CKO (Figures S1D and S1E). To determine whether these changes led to functional impairment in behavioral tasks, control and Sox17 CKO animals were tested on the inclined beam task at both P30 and P60. While the 2cm beam could not distinguish between controls and CKO, the more challenging 1cm beam revealed significant functional deficit of the Sox17 CKO at both P30 and P60 (Figure 1K; 1-cm control 0.13 ± 0.09 foot slips/trial, CKO 1.10 ± 0.23 foot slips/trial, p = 0.0002; 2-cm control 0.20 ± 0.14, CKO 0.60 ± 0.22 foot slips/trial, p = 0.13).

Sox17 Regulates OPC Expansion and Sustains Differentiation

Because the decrease in OLs occurs during active postnatal oligodendrogenesis and myelination, it is possible that Sox17 deficiency disrupted OPC differentiation and/or OPC production. NG2^{+} cells were found significantly decreased in the P18 CKO (Figures 2A and 2B). This is due to reduced proliferation, as evidenced by reduced Ki67^{+} and NG2^{+}BrdU^{+} cells (Figure 2C). To determine whether this change arose from the cell-autonomous loss of Sox17, an analysis of NG2 cell proliferation in P18 CNP-Cre$^{/+}$;Sox17$^{f/f}$;Rosa26YFP (CKO;RosaYFP) mice was performed. As shown in Figures 2D and 2E, compared with CNP-Cre$^{/+}$;Rosa26YFP, fewer yellow fluorescent protein (YFP)-expressing OPCs, or NG2^{+}YFP^{+} cells were present in the P18 CKO;Rosa26YFP WM than were bromodeoxyuridine positive (BrdU^{+}). The CNP-Cre-targeted recombination rate within the NG2 cell population was estimated at about 25% (Figures S2A and S2B). Within the YFP^{+} population, Sox17 ablation produced a significant decrease in proliferating NG2^{+} cells. Among CNP-Cre$^{/+}$;Rosa26YFP-expressing cells, the loss of Sox17 caused a decrease in the percentage of Sox2-expressing progenitor cells at P18 (Figure 2F). Sox2^{+}BrdU^{+}YFP^{+} OPCs are detectable at P18 in less intense YFP+ cells in this mouse strain (Figure S2C). When the total Sox2 population was analyzed, there was a significant decrease over postnatal WM development in the CKO (Figures 2G and 2H). This was due to reduced cell proliferation (Figures S2D–S2F).

Sox17 Ablation in OPCs Impairs OL Production

To determine whether Sox17 loss in OPCs was sufficient to produce the observed biphasic change in OLs during postnatal development, we generated CNS-progenitor-targeted Sox17 mutants by breeding *PDGFRa*CreER^{T2} with Sox17$^{f/f}$ mice. Analysis of *PDGFRa*CreER$^{T2/+}$;Sox17$^{f/f}$ (PCKO) mice over postnatal development revealed a pattern of change in the oligodendroglial lineage similar to that observed in CKO. Figure 3A shows that early postnatal ablation with tamoxifen (Tam) at P4–P6

(J) Quantitative analysis revealed decreased percentage of myelinated axons in the P60 CKO compared with CNP-Cre and Sox17$^{f/f}$ groups as separate control groups. n = 6–12.

(K) Behavior analysis using the 1-cm inclined beam test distinguishes CKO from Ctrl by increased footslips at P30 and P60, supporting abnormal WM function resulting from Sox17 deficiency. n = 6. ***p < 0.001, **p < 0.005, *p < 0.05, Student's t test versus Ctrl, mean ± SEM. Scale bars, 50 μm; except in (H) scale bars, 10 μm.

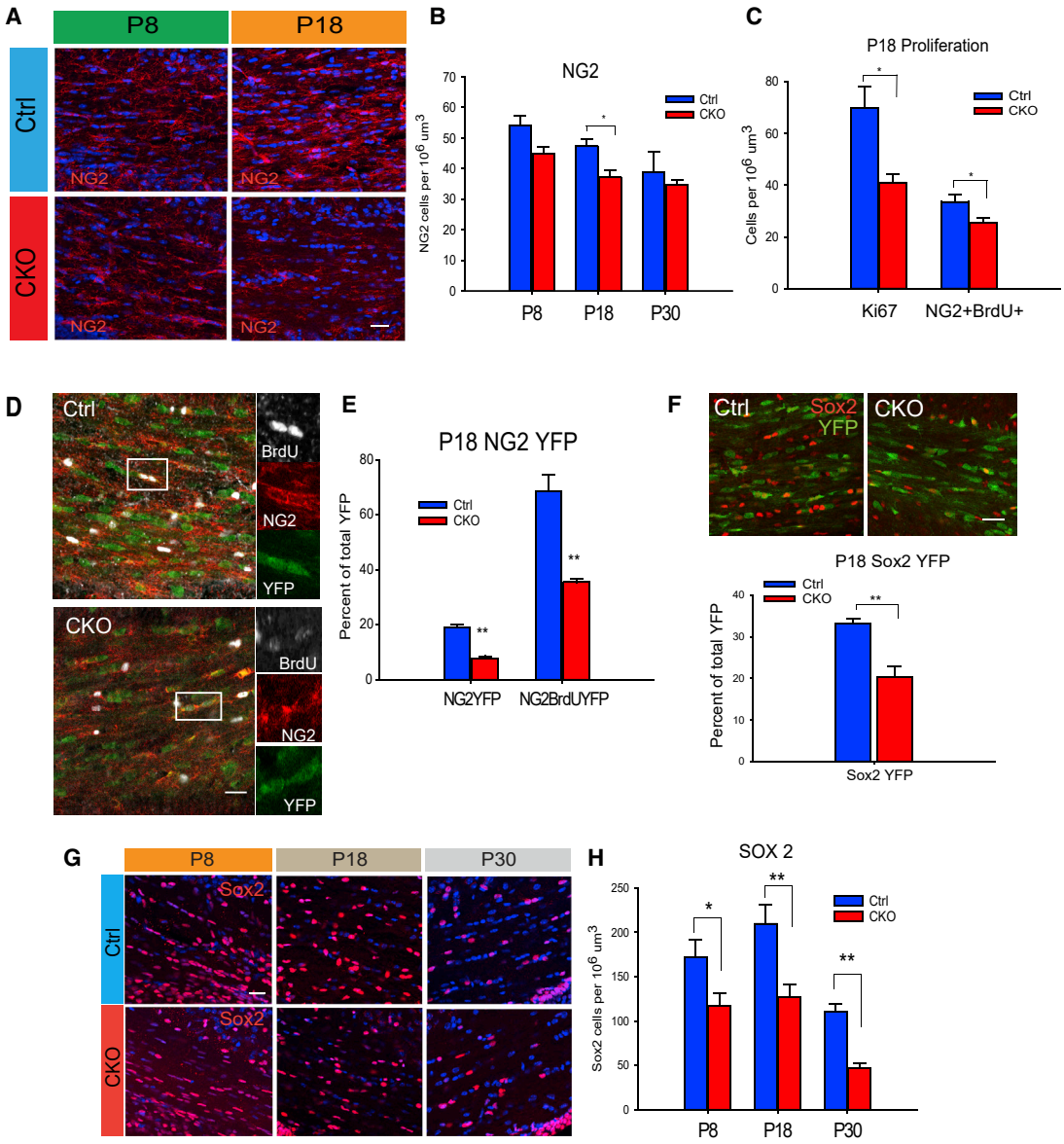

Figure 2. Sox17 Regulates OPC Expansion

(A) Immunohistochemical analysis of NG2-expressing OPCs (red) in P8 and P18 WM.

(B) Quantitation shows little change in NG2 cells of CKO at P8 but significant decrease at P18.

(C) Analysis of proliferation using Ki67 and BrdU reveals decreased Ki67 and BrdU labeling in WM at P18. n = 4. *p < 0.05 and **p < 0.005, Student's unpaired t test, mean ± SEM. A total of 50 mg/kg BrdU was injected intraperitoneally (i.p.) 24 h prior to sacrifice.

(D) Confocal microscope images of triple immunostaining for NG2 (red), CNP-Cre;RosaYFP (green) and BrdU (white) at P18. Cells in boxed areas are magnified and shown in their individual channels.

(E) Decreased total NG2- and BrdU-labeled OPCs within the CNP-Cre;RosaYFP population at P18 indicates an underlying deficit in proliferation. n = 3. *p < 0.05 and **p < 0.01, Student's unpaired t test, mean ± SEM.

(F) The number of Sox2-expressing progenitor cells is decreased in P18 CKO WM. n = 3. *p < 0.05 and **p < 0.005, Student's unpaired t test, mean ± SEM.

(G) Confocal microscope images showing Sox2-expressing cells (red) in WM at P8, P18 and P30.

(H) The total number of Sox2-expressing cells is decreased in developing WM of the postnatal CKO. n = 4 **p < 0.005, *p < 0.05, Student's t test versus Ctrl, mean ± SEM. Scale bars for (A), (D), and (F), 20 μm; for (G), 50 μm.

reduces NG2 progenitor cells at P8 without altering CC1 OLs. Subsequently, analysis at P18 shows a smaller reduction in NG2 progenitors, but this change is accompanied by an increase in CC1 OLs (Figure 3B). Tam injections at P7 were estimated by *in situ* hybridization to lead to Cre-based recombination in about 70% of PDGFRa-expressing OPCs (Figures S3A and S3B), which was sufficient to induce a detectable change in overall Sox17 expression (Figures S3C–S3E). By P28, CC1

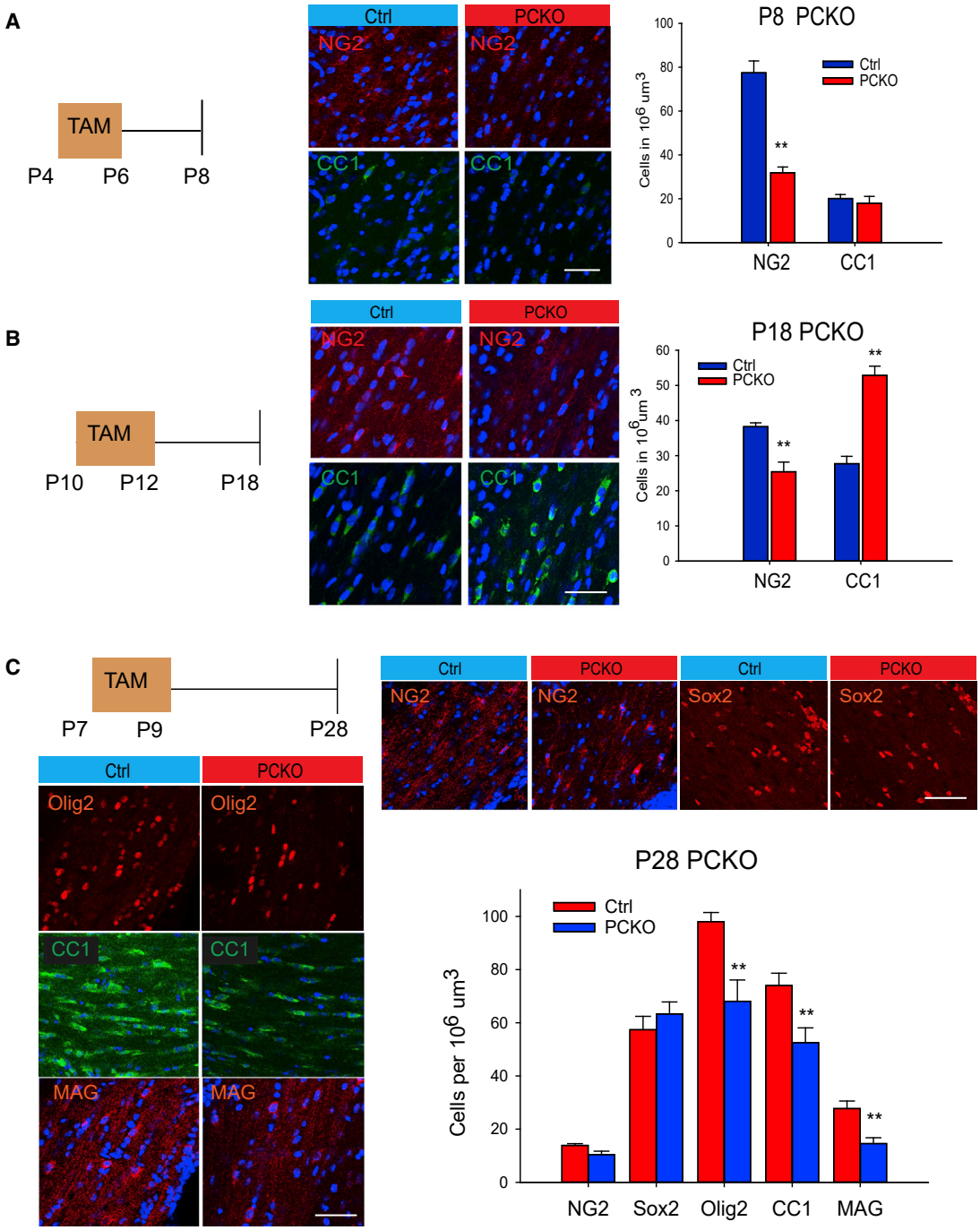

Figure 3. Sox17 Ablation in Progenitor Cells Regulates Oligodendrocytes in Biphasic Manner

(A) Tamoxifen (TAM)-induced ablation in *PDGFRa*CreER$^{T2/+}$;Sox17$^{f/f}$(PCKO) between P4 and P6 reduces NG2 (red) but not CC1 (green) in P8 WM. n = 3.

(B) TAM-induced Sox17 ablation between P10 and P12 reduces NG2 (red) and increases CC1 (green) in P18 WM. n = 3.

(C) TAM-induced Sox17 ablation between P7 and P9 reduces oligodendrocytes (OLs) in P28 PCKO WM. Significant decreases in Olig2 (red), CC1 (green), and MAG (red) OLs are observed without changes in NG2- (red) or Sox2 (red)-expressing progenitor cells. n = 3. **p < 0.005, Student's t test, mean ± SEM. Scale bars, 50 μm.

OLs are significantly reduced (Figure 3C). At this time point, the numbers of progenitor cells are no longer significantly different, based on NG2 and Sox2 cell analysis (Figure 3C). The decrease in Olig2- and MAG-expressing cells (Figure 3C) indicates a sustained disruption of differentiation despite progenitor recovery.

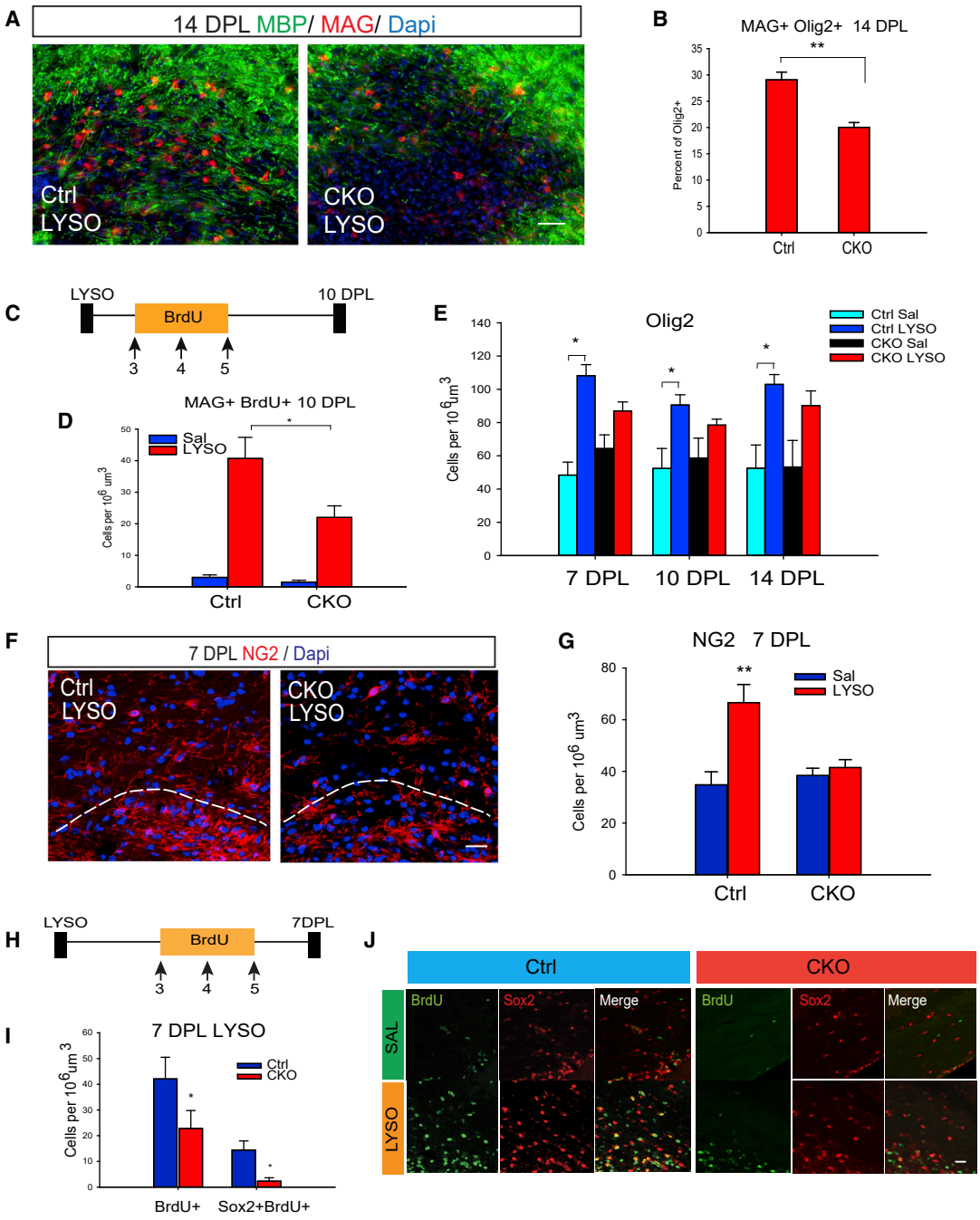

Figure 4. Sox17 Promotes Oligodendrocyte Regeneration after LPC Demyelination (LYSO)

(A) Immunohistochemical analysis showing WM lesion area in CKO at 14 DPL that remains largely devoid of MBP (green) and MAG (red) immunostaining, which indicates regenerating oligodendrocytes.

(B) Analysis of $MAG^{+}Olig2^{+}$ cells observed in the lesion area shows decreased numbers in the CKO at 14 DPL. n = 4.

(C) Schematic illustration of the labeling paradigm to determine regenerative oligodendrogenesis. A total of 50 mg/kg BrdU was injected i.p. daily from 3–5 DPL, followed by sacrifice at 10 DPL.

(D) The number of BrdU-labeled MAG cells is reduced in CKO lesions relative to control at 10 DPL. n = 4.

(E) Analysis of Olig2-expressing cells from 7–14 DPL reveals a defective oligodendroglial response in CKO lesions. n = 3.

(legend continued on next page)

Sox17 Ablation Impairs Remyelination

Given the importance of Sox2-expressing progenitor cells in both OPC proliferation and differentiation (Zhang et al., 2018), it is likely that Sox17 control of Sox2 and NG2 cell populations impacts progenitor-dependent cell regeneration following injury in the adult WM. To determine whether Sox17 ablation impedes OL regeneration in demyelinating lesions, LPC or lysolecithin (LYSO)-induced focal demyelination lesions in the P60 cingulate WM were analyzed. The density of MAG^+ cells labeled by cytoplasmic staining was significantly lower in the CKO at 14 days post lesion (DPL) (Figures 4A and 4B). At 10 DPL, MAG cells were reduced in CKO lesions (Ctrl 22.36 ± 2.41 versus CKO 15.52 ± 1.55 per 10^6 μm^3, $p < 0.05$, Student's unpaired t test), and BrdU pulse labeling (Figure 4C) revealed fewer newly formed MAG^+ cells in CKO lesions (Figure 4D). The diminished response of Olig2 cells in CKO lesions (Figure 4E) suggests altered induction or activation of OPCs. Indeed, the production of NG2 cells in response to demyelination at 7 DPL was deficient in the CKO (Figures 4F and 4G). Similar to development, Sox17 ablation diminished the demyelination-induced increase in $BrdU^+$ cells, including regenerative Sox2-expressing cells in WM at 7 DPL (Figures 4H–4J).

Sox17 Regulates the Notch Signaling Pathway That Controls OL Progenitor Expansion

To understand mechanisms that underlie Sox17 regulation of OL formation in the WM, we sought to determine the expression of factors that control progenitor cell expansion and maturation, such as Sox2 (Zhang et al., 2018) and TCF7L2 (Hammond et al., 2015; Zhao et al., 2016). Figure 5A shows that Sox17 knockdown in cultured OPCs revealed a surprisingly selective effect on TCF7L2 protein, rather than on Sox2. This selectivity was confirmed at the RNA level by quantitative PCR (Figure 5B). We hypothesized that because Sox17 did not regulate Sox2 expression in OPCs, its control of the Sox2 cells could be mediated through signaling, which regulates the progenitor population (Zhang et al., 2009), such as Notch. Indeed, the protein levels of cleaved or activated Notch1 (Act N1; Figure 5A) and RNA levels of Notch1 receptor and signaling effectors Hes1 and Hes5 were significantly reduced by Sox17 siRNA (Figure 5B). To determine whether Notch signaling regulated TCF7L2 or Sox2 gene expression in cultured OPCs, we applied the gamma secretase inhibitor N-[(3,5-Difluorophenyl)acetyl]-L-alanyl-2-phenyl] glycine-1,1-dimethylethyl ester (DAPT) for 2–3 days and found that TCF7L2 RNA was reduced, whereas Sox2 remained unaffected (Figure 5C). Notch1 was found to mediate this change in TCF7L2 expression because Notch1 small interfering RNA (siRNA) transfection of cultured OPCs also decreased TCF7L2 without affecting Sox2 RNA (Figure 5D). DAPT decreased the percentage of proliferating Sox2 cells in culture (Figure 5E-F), ultimately decreasing the total number of Sox2 cells (Figure S4A), indicating that Notch regulates the expansion of Sox2-expressing OPCs, rather than its expression. Although 1 μM and 2 μM DAPT were found to reduce cell viability to a similar extent (Figure S4B), 1 μM was selected for subsequent assays analyzing differentiation (below).

Based on Sox17-induced changes in Notch1 expression, we investigated the possibility that Sox17 might interact with a Notch1 enhancer region in developing WM. A recent study of SoxF factors by Chiang et al. (2017) in arterial development identified two Sox consensus-containing intronic enhancers within the Notch1 gene that bound recombinant Sox7 and Sox18. Using these sequences as electrophoretic mobility shift assay (EMSA) probes, we found that the sequence corresponding to HmSox-a (Chiang et al., 2017), which we call SoxA in this study, formed a sequence-specific complex with nuclear proteins from P12 WM (Figures 5G and 5H), whereas HmSox-b or SoxB did not. Figure 5I shows that the complex is vulnerable to disruption by anti-Sox17 antibody, indicating the presence of Sox17 in this complex from WM. To determine whether Sox17 in proliferating OPCs bound the SoxA sequence, we performed EMSA analysis by using nuclear extract isolated from rat OPCs cultured for 2 days in platelet-derived growth factor (PDGF). Figures 5J shows that a SoxA-specific complex was detected that was disrupted by Sox17 antibodies from two vendor sources (Figure 5K; antibody S1 and S2). These data are consistent with the notion of direct control of Notch1 expression by Sox17 that could underlie progenitor cell expansion.

To determine whether Notch signaling *in vivo* was altered by Sox17 loss, the number of WM cells expressing Notch mediators Hes1 and Hes5 was analyzed. These were decreased in CKO WM at P8 and P18 (Figures 5L and 5M). Hes1 distribution at P18 was not exclusively nuclear, unlike Hes5 at P8 (Figure 5N), but total Hes1- and Hes5-expressing cells were decreased in number in CKO (Figure 5P). We then determined whether Notch1 activation was regulated in CNP-Cre-targeted cells. Figure 5Q shows that in P18 controls, CNP-Cre-targeted YFP reporter expression (green) was colocalized with activated Notch1(ActN1, red). The percentage of YFP cells that colocalized with ActN1 was significantly decreased (Figure 5R), indicating that Sox17 ablation cell autonomously downregulated Notch1 activation in P18 CKO WM.

TCF7L2 Is Regulated by Sox17 and Notch Signaling

Given the function of Notch in progenitor maintenance, the biphasic change in TCF7L2 cells of the developing CKO WM (Figures 6A and 6B) suggests bona fide changes in differentiation events—disrupted progenitor expansion and enhanced precocious differentiation, followed by unsustained differentiation and eventual OL reduction. Progenitor-targeted Sox17 ablation reproduced the biphasic change in TCF7L2-expressing cells between P18 and P28 (Figures 6C and S5). We wanted to

(F and G) Confocal images (F) and quantification of NG2 cells (G) in WM lesions at 7 DPL showing reduced numbers of NG2 cells (red) populating the CKO subcortical WM region adjacent to the subventricular area delineated by the white dashed line. Quantification reveals the absence of a significant progenitor cell response to demyelination in CKO. n = 3. **p < 0.005, ANOVA, Holm-Sidak post hoc test.

(H) Schematic representation of BrdU-labeling paradigm followed by sacrifice at 7 DPL.

(I and J) Quantified immunohistochemical analysis (I) and confocal microscope images (J) of subcortical WM lesions showing decreased numbers of BrdU-labeled (green) Sox2-expressing cells (red) in the CKO. n = 3. Scale bars in (A), 50 μm; (F) and (J), 20 μm. **p < 0.005, *p < 0.05, Student's t test versus Ctrl., mean ± SEM.

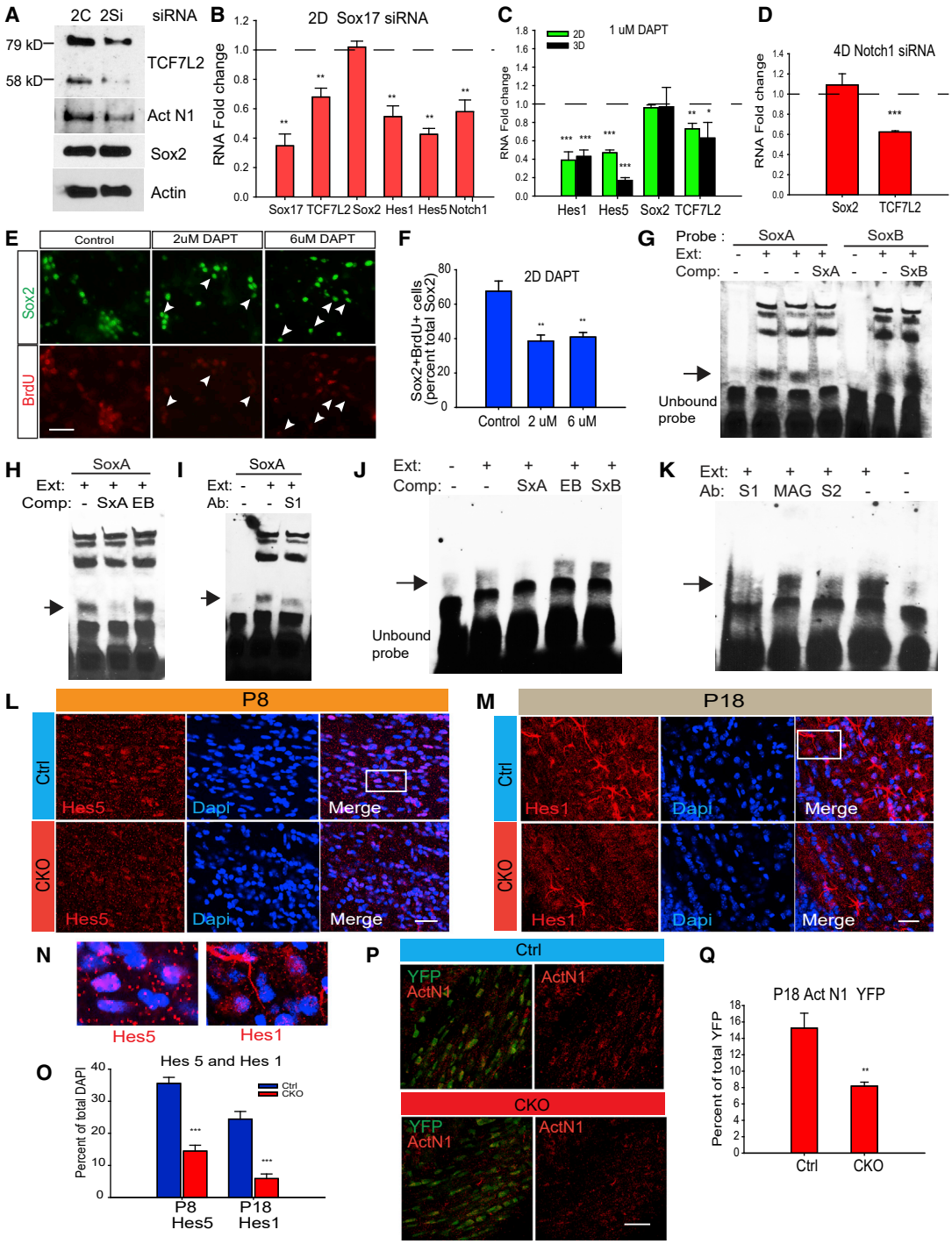

Figure 5. Sox17 Regulates Oligodendroglial Notch Signaling

(A) Western blots of cultured OPCs transfected with siRNA and analyzed 2 days after transfection. Sox17 siRNA (2S) reduces activated Notch1 (Act N1) and both bands of TCF7L2 protein, not Sox2, when compared with control siRNA (2C). n = 2.

(B) Quantitative real-time PCR analysis showing OPC RNA changes in TCF7L2, Notch1, and Hes genes after 2 days of Sox17 siRNA transfection. n = 4.

(C) Quantitative PCR analysis showing RNA changes in Hes genes and TCF7L2 following 2 and 3 days treatment of OPCs with 1 μM DAPT. n = 4.

(D) qPCR analysis showing decreased TCF7L2 and not Sox2RNA after 2 days of Notch1 siRNA transfection.

(E) Images of cultured OPCs immunostained for Sox2 (green) and BrdU (red) after 2 days co-treatment with PDGF and 2 μM or 6 μM DAPT. 50 μM BrdU was added 12 h before analysis. Arrowheads indicate Sox2 cells with weak or no BrdU labeling.

(F) The percentage of Sox2 cells labeled with BrdU was decreased after DAPT treatment. n = 3. Scale bar, 50 μm. *p < 0.05, **p < 0.01, ***p < 0.005, Student's unpaired t test, mean ± SEM.

(legend continued on next page)

determine whether Sox17 also similarly regulated TCF7L2 in OL regeneration. In the intact adult WM, TCF7L2 is undetectable (Zhao et al., 2016), but its upregulation upon demyelination is dependent on Sox17 (Figures 6D and 6E). As in CKO development, the change in total TCF7L2-expressing cells undergoes an initial increase at 7 DPL, followed by decrease at 10 DPL (Figure 6F). BrdU pulse-labeling showed fewer newly formed TCF7L2 cells in the CKO by 10 DPL (Figure 6G). It is possible that the initial increase in TCF7L2 lies downstream of Notch inhibition, as cultured OPCs treated with DAPT also show enhanced differentiation based on increased O4 and TCF7L2-expressing cells (Figures 6H and 6I). Together, the observations are consistent with the interpretation that TCF7L2 may contribute to Sox17 functions in differentiation, and thus Sox17 regulates the number of OLs in the adult WM through progenitor expansion and subsequent differentiation.

Sox17 Function in Adult OPCs Regulates Oligodendroglial Response to Demyelination

To determine whether Sox17 ablation in adult OPCs regulated oligodendroglial regeneration, we performed LPC lesions in P60 PCKO mice, which received Tam injections 3 days prior to demyelination (Figure 7A). At 7 DPL, the number of NG2 progenitor cells was attenuated in PCKO (Figures 7B and 7C), accompanied by decreased ActN1 (Figures 7D and 7E). Lesion-induced Sox2-expressing oligodendroglial lineage cells, which co-express YFP reporter in controls (Figure S6A), were found to be significantly reduced in PCKO lesions along with Hes1 (Figures S6B and S6C). Olig2 cells were decreased in PCKO lesions, indicating an impaired oligodendroglial cell response (Figures 7F and 7G). The increased numbers of lightly stained Olig2 cells in intact PCKO may be due to progenitor maturation (Figure 7G, Sal). These observations support the interpretation that Sox17 in OPCs controls Notch1 activation, which enhances progenitor cell expansion in response to demyelination.

Notch Inhibition in Adult Sox17-Overexpressing WM Decreases Progenitor Cells

To determine whether Sox17 gain-of-function *in vivo* increases the progenitor cell population through Notch, we analyzed adult CNPSox17 transgenic mice at P60 when Ctrl progenitor proliferation had declined. This transgenic strain, which overexpresses recombinant, full-length mouse Sox17 in NG2, O4, and CC1 cells of subcortical WM, displays increased numbers of OLs in adult WM (Ming et al., 2013). Figures S7A and S7B show that Sox2-expressing cells in the intact CNPSox17 WM were significantly increased over Ctrl (saline), consistent with previous findings of greater numbers of NG2-expressing cells (Ming et al., 2013). Following LPC demyelination, at 3DPL—before the well-defined peak of progenitor proliferation in Ctrl mice reported to be at 7 days (Aguirre et al., 2007; Nait-Oumesmar et al., 1999; Watanabe et al., 2002; Woodruff and Franklin, 1999)—the CNPSox17 mouse showed an additional Sox2 cell response that was absent in Ctrl (Figure S7B). Sox17 overexpression was also previously shown to elevate the numbers of TCF7L2 cells (Ming et al., 2013). Our observation that WM lesions selectively stimulated an increase in TCF7L2 cells only in WT mice (Figure S7C) suggests that signaling mechanisms upregulating TCF7L2 and Sox2 cells in the CNPSox17 mouse were already intrinsically stimulated. Figure 7H shows that ActN1 is elevated in intact P60 CNPSox17 WM over WT controls. A single stereotaxic injection of 50 μM DAPT significantly reduced ActN1 levels in CNPSox17 (Figure 7H). To determine whether the increased population of NG2- and Sox2-expressing cells in the intact adult CNPSox17 transgenic WM was produced by enhanced Notch signaling, the numbers of NG2 and Sox2 cells were analyzed after stereotaxic injection of 50 μM DAPT (Figures 7I and 7J). These experiments showing a reduction of NG2 and Sox2 cells in the CNPSox17 WM by DAPT implicate Notch signaling in progenitor maintenance. In Lyso lesions of the CNPSox17, this dose of DAPT was effective in decreasing lesion-induced ActN1, NG2, and Sox2 cells and increasing OPC differentiation, indicated by Olig2 and CC1 cells at 3 DPL (Figures S7D and S7E). Taken together, our studies provide evidence of a programmatic role for Sox17 in the control of Notch expression and in OL production through progenitor expansion and subsequent differentiation.

DISCUSSION

Sox factors control many aspects of development in OLs, ranging from lineage specification to effects on proliferation and survival, with the majority of the literature focused on the SoxD and SoxE families. SoxF factors are involved in hematopoietic progenitor regulation (He et al., 2011), tumor angiogenesis (Yang et al., 2013), and arterial development (Chiang et al., 2017). To date, Sox17 is the only SoxF family member whose expression has been shown to be developmentally regulated in postnatal WM, and the physiological function of endogenous Sox17 within OLs *in vivo* is poorly understood. This study demonstrates that Sox17 contributes to the size of the WM OL population by

(G–I) EMSA analysis with P12 WM extract (Ext) shows sequence-specific complex formation on a Sox binding sequence (SoxA) probe derived from the Notch1 intron. (G) Sequence-specific complexes do not form on SoxB probe. SxA is the unlabeled competitor oligo for SoxA and SxB for SoxB. (H) Using SoxA as probe, unrelated oligonucleotide sequence EBNA (EB) fails to competitively disrupt the complex on SoxA. (I) With SoxA as probe, Sox17-specific antibodies (S1) disrupt the SoxA complex. All arrowheads indicate position of Sox17-specific DNA-protein complex.

(J and K) EMSA analysis using OPC nuclear extracts with SoxA probe. (J) SxA competitor (Comp) successfully abolishes complex formation by OPC nuclear extract (Ext) but not EB or SxB. (K) Antibodies (Abs) against Sox17 (S1 and S2) reduce complex formation on SoxA probe, whereas MAG antibody is without effect.

(L) Confocal microscope images showing Hes5-expressing cells (red) at P8. (M) Confocal microscope images showing Hes1-expressing cells (red) at P18. Note the numbers of 4′,6′-diamidino-2-phenylindole (DAPI) nuclei are comparable in Ctrl and CKO.

(N) Magnified views of boxed areas in (L) and (M) showing cellular distribution of Hes proteins. Hes1 is less nuclear.

(O) Quantitation shows that total Hes5 and Hes1 cells are decreased by Sox17 ablation.

(P and Q) Act N1(red) levels are decreased in YFP reporter cells (green) of CKO at P18. n = 3. Scale bars, 50 μm except in (D) where scale bar, 20 μm **$p < 0.01$, ***$p < 0.005$. ANOVA Holm-Sidak posthoc (D) or Student's unpaired t test (F). mean ± SEM.

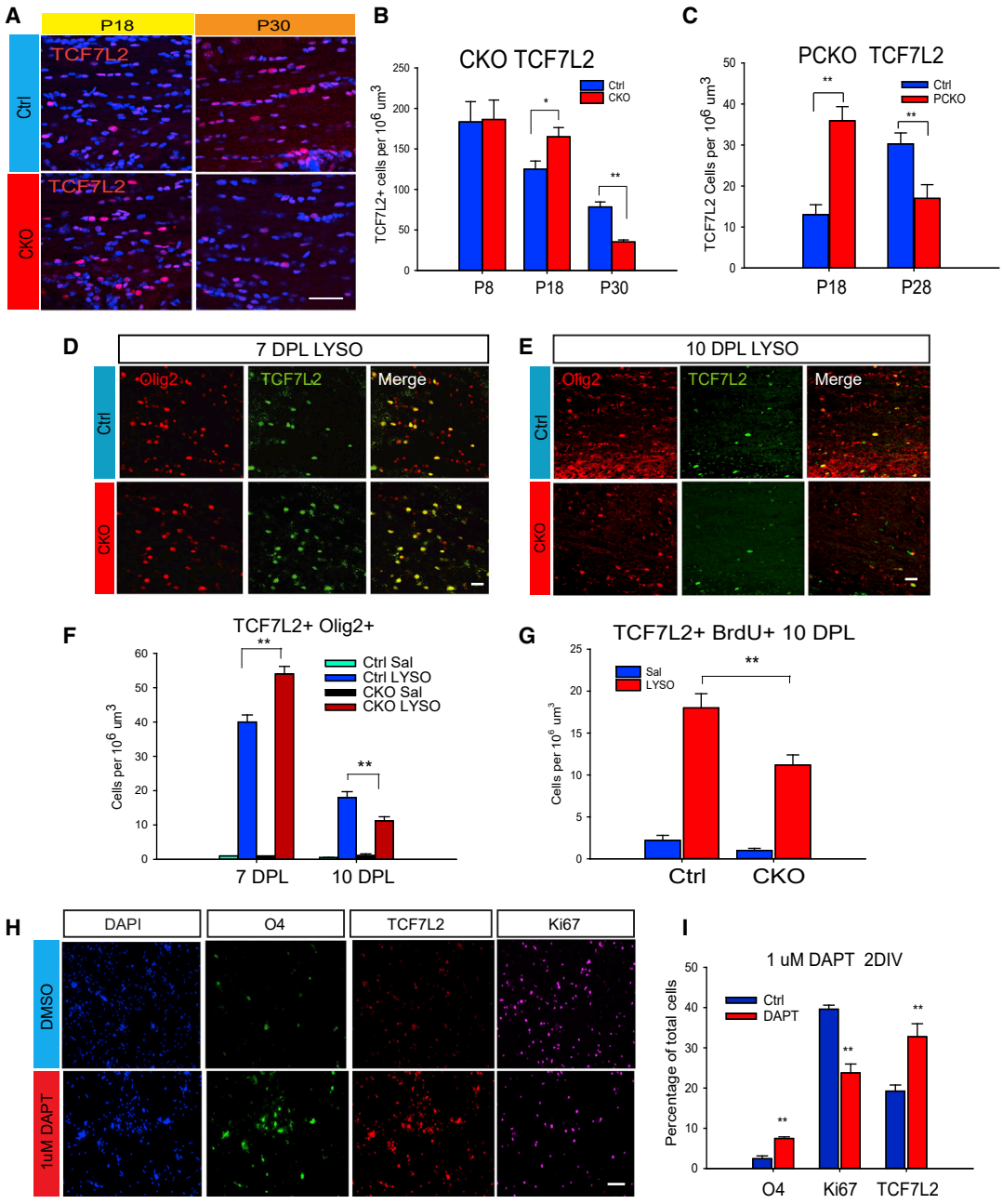

Figure 6. Biphasic Regulation of TCF7L2-Expressing Cells by Sox17

(A) Confocal microscope images showing TCF7L2-expressing cells (red) in WM at P18 and P30. (B) Quantitation showing biphasic change in TCF7L2-expressing cells in developing CKO WM, consistent with premature and transiently increased differentiation. Scale bar, 50 μm.

(C) Sox17 ablation in PCKO causes biphasic changes in TCF7L2-expressing cells during WM development. TAM was administered as in Figures 3B and 3C.

(D) Confocal microscope images showing Olig2 (red) and TCF7L2 (green) cells following LPC demyelination (LYSO) at 7 DPL. (E) Confocal microscope images showing Olig2 (red) and TCF7L2 (green) cells following LPC demyelination (LYSO) at 10 DPL. Scale bars, 20 μm.

(F) Cell quantification showing increased TCF7L2$^+$Olig2$^+$ cells in CKO lesions at 7 DPL, whereas decreased numbers are observed at 10 DPL. n = 3.

(G) Reduced BrdU pulse labeling in CKO at 3–5 DPL indicates that Sox17 promotes the generation of TCF7L2-expressing cells at 10 DPL.

(H) Images of cultured OPCs immunostained for O4 (green), TCF7L2 (red) and Ki67 (magenta) after exposure to 1 uM DAPT for 2 days under proliferating conditions. (I) Exposure of proliferating OPC cultures to 1 μM DAPT for 2 days decreases the percentage of Ki67 proliferating cells and increases the proportion of differentiating cells expressing O4 and TCF7L2. Scale bar, 50 μm. n = 4. **$p < 0.01$, Student's unpaired t test, mean ± SEM.

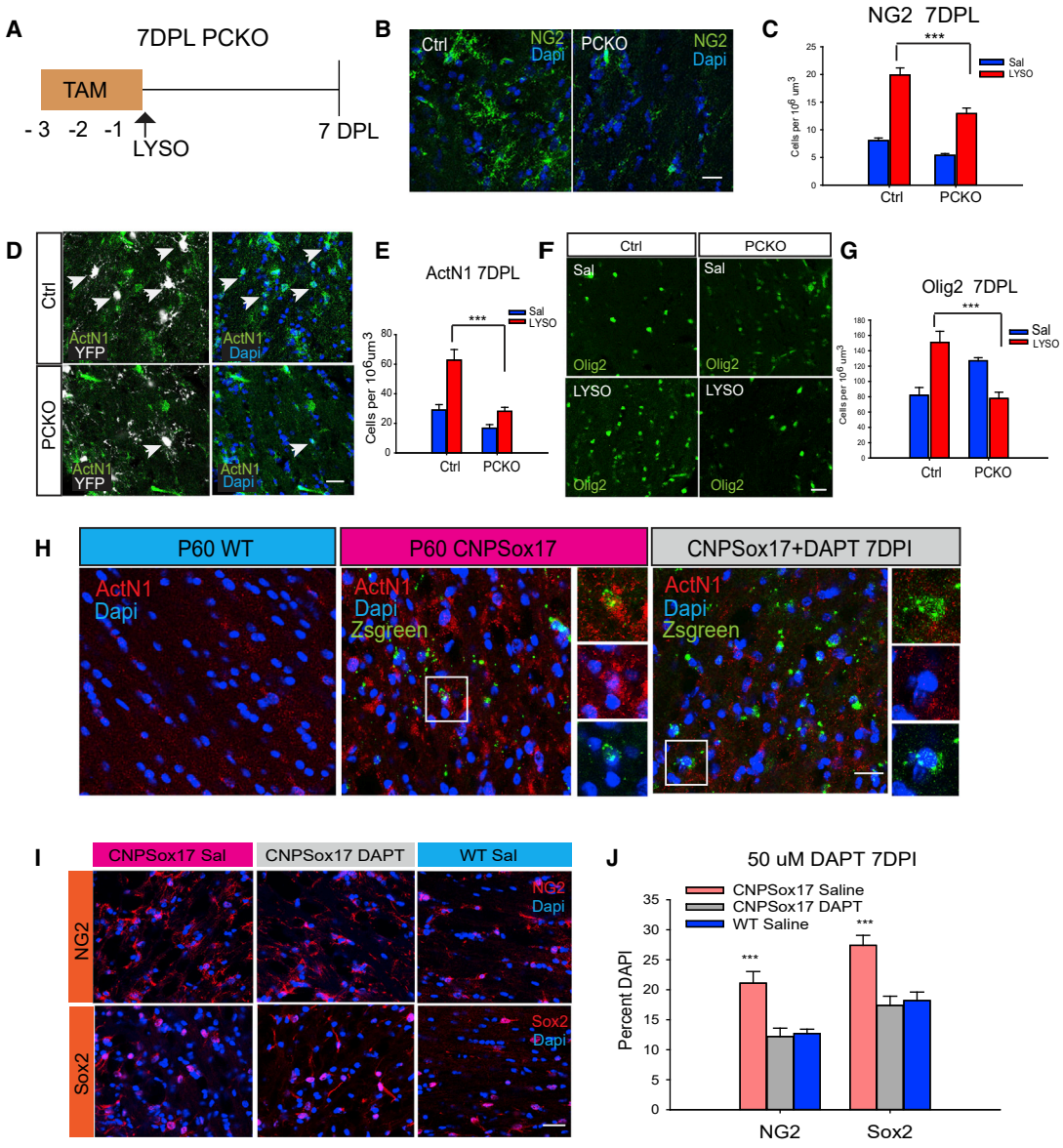

Figure 7. Adult OPC Regulation by Sox17 Involves Notch

(A) Illustration of daily TAM injections and demyelination paradigm (LYSO) in PCKO. Analysis was performed at 7 DPL.

(B) Confocal microscope images showing LYSO lesions with NG2 (green) progenitor cells in Ctrl and PCKO at 7 DPL. (C) Quantitative analysis showing an attenuated NG2 cell response in PCKO.

(D) Confocal microscope images showing LYSO lesions with activated Notch1 (ActN1, green) in YFP progenitor cells (white). (E) Quantitative analysis showing decreased ActN1 in LYSO lesions of PCKO. Arrowheads indicate nuclear ActN1 (green) colocalized with Rosa26YFP reporter (white).

(F) Images showing Olig2 cells (green) in intact (Sal) and lesioned (LYSO) WM at 7 DPL. (G) Sox17 ablation decreases Olig2 (green) cells at 7 DPL.

(H) Activated Notch1 (ActN1, red) is increased in intact WM of P60 CNPSox17 transgenic mice relative to WT. Inset shows a Zsgreen reporter (green)-expressing cell colocalized with ActN1(red). Notch inhibition in WM of P60 CNPSox17 mice with 50 μM DAPT decreases Notch activation (ActN1, red) at 7 days post injection (DPI).

(I) Images showing NG2(red) and Sox2(red) cells in intact WM and the effect of 50 uM DAPT injection in CNPSox17 WM at 7DPI. (J) DAPT decreases mean percentages of NG2 and Sox2 progenitor cells (red) to WT levels at 7 DPI. n = 3. Scale bars, 20 μm. *p < 0.05, **p < 0.01, ***p < 0.005, ANOVA Holm-Sidak posthoc (C, E, G, and J). mean ± SEM.

promoting a program of OPC expansion and maturation that impacts both myelination and functional behavior.

Our laboratory has previously reported pro-differentiation functions of Sox17 in cultured OPCs (Chew et al., 2011; Sohn et al., 2006). Sox17 expression is lower in progenitor cells and mature OLs and peaks at the intermediate O4 stage (Sohn et al., 2006). Although the significant decline in OL number was not surprising in CKO WM, the detection of biphasic Olig2 cell

changes and precocious differentiation was unanticipated. The observations reflect the temporal and spatial pattern of Sox17 expression in the lineage, with greater and more persistent loss of OLs than OPCs. In regulating multiple stages of the oligodendroglial lineage, Sox17 appears to stand apart from the better-established SoxE members. Sox9 critically specifies OPCs, but its loss does not affect Olig2 cells in the spinal cord (Stolt et al., 2003). Although both Sox17 and Sox10 regulate myelin genes (Sohn et al., 2006), Sox17 ablation *in vivo* leads to a deficit in OPCs in CKO and PCKO, an effect not reported with Sox10 loss (Stolt et al., 2002). The decrease in OPCs labeled with ROSA26YFP following Sox17 loss in CKO indicates that cell-autonomous Sox17 activity contributes to the proliferation and maintenance of the OPC population. Indeed, the change in $Sox2^{+}$;$Rosa26YFP^{+}$ cells during postnatal development supports this interpretation. Our findings using a time-course series of Tam-induced ablation of Sox17 in developing PCKO (Figure 3) indicate that the biphasic pattern of OL changes is initiated at the level of the OPC. This suggests that the changes in CKO could also have been initiated at the level of the OPC, despite broader expression of the CNP-Cre. Although Sox2 also labels adult glial fibrillary acidic protein (GFAP)-expressing astrocytes (Zhao et al., 2015), we detect Sox2 in cells that co-express Rosa26YFP reporter in LYSO lesions of adult *PDGFRa*$CreER^{T2/+}$;Rosa26YFP mice, arguing that a population of adult Sox2-expressing OPCs (Zhang et al., 2018) may be responsible for the oligodendroglial responses observed in the absence of Sox17.

Although our current findings of Sox17 in progenitor expansion appear to be at odds with our previous reports of Sox17 in OPC differentiation (Chew et al., 2011; Sohn et al., 2006), it should be noted that these studies were primarily performed in cultured cells maintained under highly proliferating conditions. It is possible that transient effects on OPC expansion in this system would be less readily detectable than lasting effects on differentiation. Emerging evidence from studies of Sox proteins indicate that changes in both progenitor cells and mature OLs can result from the loss of a single factor. Sox2 not only possesses "stem-ness" properties (Zhao et al., 2015) but also promotes progenitor proliferation and differentiation (Hoffmann et al., 2014; Zhang et al., 2018; Zhao et al., 2015). It is presently not clear how TCF7L2-expressing cells are regulated by Sox17 ablation. As a differentiation factor, Sox2 is known to be upregulated in TCF7L2-expressing newly formed OLs (Hammond et al., 2015; Zhang et al., 2018). We do observe an increase in Sox2 intensity despite reduced Sox2 cell number in Sox17 mutants; suggesting Sox2 involvement in early differentiation events in parallel with TCF7L2 (Zhao et al., 2016). It is possible that the subsequent accelerated death of CKO CC1 cells arises from the lack of secondary or indirect targets of Sox17 that promote progenitor differentiation. Although progenitor depletion can contribute to the mechanism of OL loss, our observation of substantial NG2 cell recovery in Sox17 mutants argues that other processes initiated in OPCs, such as differentiation and survival, are likely to be involved in the functions of Sox17 in this lineage. Our studies showing regulation of TCF7L2 support the notion of a differentiation target of Sox17 and of Notch, although future studies will determine its underlying molecular mechanisms.

Both Sox2 and TCF7L2 have been reported to be regulated by canonical Notch signaling in neural stem cells (Li et al., 2012); however, less is known about their functional relationships in OPCs. Sox17 overexpression increases the number of WM cells expressing TCF7L2/TCF4 (Ming et al., 2013). Our evidence shows that Sox17 regulates TCF7L2 gene expression in OPCs along with Notch1 receptor and that DAPT and Notch1 siRNA also decrease TCF7L2 RNA. These findings suggest a requirement for Notch1 signaling in TCF7L2 control by Sox17. Together with the previous observation that Notch1 signaling supports OPC proliferation (Zhang et al., 2009), our results are consistent with the notion that Sox17 contributes to developmental OPC expansion by regulating Notch signaling. Indeed, we have identified a Notch1 enhancer as a binding target of Sox17 in developing WM and in proliferating OPCs, which provides support for direct control by Sox17. We also found Notch-related genes among differentially expressed genes from microarray analysis after Sox17 siRNA knockdown in cultured OPCs, a paradigm that dysregulates Wnt and differentiation (Chew et al., 2011; data not shown). Interestingly, Notch targets were not identified by RNA sequencing (RNA-seq) screening using a gain-of-function approach by inducible Sox17 overexpression in oligodendroglial cells (Fauveau et al., 2018), a paradigm that led to severe developmental hypomyelination. Nevertheless, loss-of-function studies suggest that a Notch-dependent mechanism may be shared among SoxF factors in different tissue systems, as SoxF controls Notch receptor expression in arterial specification (Chiang et al., 2017). Although Sox2 has been identified as a bona fide binding target for the Notch DNA-binding cofactor, recombination signal binding protein for immunoglobulin kappa J region (RBPJ), in neural stem cells (Li et al., 2012), we have failed to observe acute regulation of Sox2 RNA and protein in cultured OPCs by Sox17 knockdown or Notch inhibition. This suggests a context-specific relationship between Notch1 and Sox2, whose effects on progenitor development are mediated by distinct mechanisms (Holmberg et al., 2008). These results nonetheless support the interpretation that Sox17 regulates the progenitor cell population at least partly through Notch signaling in WM tissue. Given the complexity of Notch functions, it is tempting to speculate that its many lineage-relevant signaling activities (Stasiulewicz et al., 2015; Yabut et al., 2015) may underlie downstream OL changes resulting from Sox17 loss.

Our studies provide *in vivo* evidence that Sox17 controls the size of the OL cell population through progenitor expansion and maturation in both WM development and regeneration. Although its regulatory functions in relation to other SoxE and SoxF family members in this cell lineage await further analysis, our findings demonstrate that by regulating the expression of a Notch receptor and its targets, Sox17 functions in a complex transcription factor network to coordinate a program of cell production and tissue homeostasis.

STAR★METHODS

Detailed methods are provided in the online version of this paper and include the following:

- KEY RESOURCES TABLE
- LEAD CONTACT AND MATERIALS AVAILABILITY

SUPPLEMENTAL INFORMATION

Supplemental Information can be found online at https://doi.org/10.1016/j.celrep.2019.10.121.

ACKNOWLEDGMENTS

This work was supported by the National Multiple Sclerosis Society grants RG4706A4/2 and RR-1512-07066 (V.G. and B.N.-O.) and partially supported by FISM 2015/R/13 (V.G.) and VA I01BX002565-05 (J.D.). Confocal and fluorescence microscopy and neurobehavioral analysis portions of this project were performed in the Neuroimaging and Neurobehavior Cores, supported by award number 1U54HD090257 from the National Institutes of Health (NIH), District of Columbia Intellectual and Developmental Disabilities Research Center (DC-IDDRDC) Award (V.G.). Its contents are solely the responsibility of the authors and do not represent the official views of the DC-IDDRC or the NIH. Further support was provided through the Fondation pour la Recherche sur la Sclérose en Plaques (ARSEP-R13008DD, B.N.-O.), the "Investissements d'avenir" ANR-10-IAIHU-06 (IHU-A-ICM) and ANR-11-INBS-0011 (NeurATRIS) to B.N.-O.

AUTHOR CONTRIBUTIONS

Conceptualization, L.-J.C. and V.G.; Methodology, L.-J.C., X.M., B.M., E.H., M.F., B.N.-O., M.C., and V.G.; Investigation and Data Analysis, L.-J.C., B.M., E.H., X.M., J.D., M.C., M.F., B.N.-O., and V.G.; Original Draft and Visualization, L.-J.C., B.M., E.H., and V.G.; Manuscript Preparation, L.-J.C. and V.G.; Funding Acquisition, L.-J.C., V.G., and B.N.-O.; Supervision, V.G.

DECLARATION OF INTERESTS

The authors declare no competing interests.

Received: June 28, 2018
Revised: May 7, 2019
Accepted: October 29, 2019
Published: December 3, 2019

REFERENCES

Aguirre, A., Dupree, J.L., Mangin, J.M., and Gallo, V. (2007). A functional role for EGFR signaling in myelination and remyelination. Nat. Neurosci. *10*, 990–1002.

Brooks, S.P., and Dunnett, S.B. (2009). Tests to assess motor phenotype in mice: a user's guide. Nat. Rev. Neurosci. *10*, 519–529.

Carter, R.J., Morton, J., and Dunnett, S.B. (2001). Motor coordination and balance in rodents. Curr Protoc Neurosci *Chapter 8*, Unit 8.12.

Chew, L.J., and Gallo, V. (2009). The Yin and Yang of Sox proteins: Activation and repression in development and disease. J. Neurosci. Res. *87*, 3277–3287.

Chew, L.J., Shen, W., Ming, X., Senatorov, V.V.J., Jr., Chen, H.L., Cheng, Y., Hong, E., Knoblach, S., and Gallo, V. (2011). SRY-box containing gene 17 regulates the Wnt/β-catenin signaling pathway in oligodendrocyte progenitor cells. J. Neurosci. *31*, 13921–13935.

Chiang, I.K., Fritzsche, M., Pichol-Thievend, C., Neal, A., Holmes, K., Lagendijk, A., Overman, J., D'Angelo, D., Omini, A., Hermkens, D., et al. (2017). SoxF factors induce Notch1 expression via direct transcriptional regulation during early arterial development. Development *144*, 2629–2639.

Fauveau, M., Wilmet, B., Deboux, C., Benardais, K., Bachelin, C., Temporão, A.C., Kerninon, C., and Nait Oumesmar, B. (2018). SOX17 transcription factor negatively regulates oligodendrocyte precursor cell differentiation. Glia *66*, 2221–2232.

Ghiani, C.A., Eisen, A.M., Yuan, X., DePinho, R.A., McBain, C.J., and Gallo, V. (1999a). Neurotransmitter receptor activation triggers p27(Kip1)and p21(CIP1) accumulation and G1 cell cycle arrest in oligodendrocyte progenitors. Development *126*, 1077–1090.

Ghiani, C.A., Yuan, X., Eisen, A.M., Knutson, P.L., DePinho, R.A., McBain, C.J., and Gallo, V. (1999b). Voltage-activated K+ channels and membrane depolarization regulate accumulation of the cyclin-dependent kinase inhibitors p27(Kip1) and p21(CIP1) in glial progenitor cells. J. Neurosci. *19*, 5380–5392.

Gubbay, J., Collignon, J., Koopman, P., Capel, B., Economou, A., Münsterberg, A., Vivian, N., Goodfellow, P., and Lovell-Badge, R. (1990). A gene mapping to the sex-determining region of the mouse Y chromosome is a member of a novel family of embryonically expressed genes. Nature *346*, 245–250.

Hammond, E., Lang, J., Maeda, Y., Pleasure, D., Angus-Hill, M., Xu, J., Horiuchi, M., Deng, W., and Guo, F. (2015). The Wnt effector transcription factor 7-like 2 positively regulates oligodendrocyte differentiation in a manner independent of Wnt/β-catenin signaling. J. Neurosci. *35*, 5007–5022.

He, S., Kim, I., Lim, M.S., and Morrison, S.J. (2011). Sox17 expression confers self-renewal potential and fetal stem cell characteristics upon adult hematopoietic progenitors. Genes Dev. *25*, 1613–1627.

Hoffmann, S.A., Hos, D., Küspert, M., Lang, R.A., Lovell-Badge, R., Wegner, M., and Reiprich, S. (2014). Stem cell factor Sox2 and its close relative Sox3 have differentiation functions in oligodendrocytes. Development *141*, 39–50.

Holmberg, J., Hansson, E., Malewicz, M., Sandberg, M., Perlmann, T., Lendahl, U., and Muhr, J. (2008). SoxB1 transcription factors and Notch signaling use distinct mechanisms to regulate proneural gene function and neural progenitor differentiation. Development *135*, 1843–1851.

Kanai-Azuma, M., Kanai, Y., Gad, J.M., Tajima, Y., Taya, C., Kurohmaru, M., Sanai, Y., Yonekawa, H., Yazaki, K., Tam, P.P.L., and Hayashi, Y. (2002). Depletion of definitive gut endoderm in Sox17-null mutant mice. Development *129*, 2367–2379.

Lappe-Siefke, C., Goebbels, S., Gravel, M., Nicksch, E., Lee, J., Braun, P.E., Griffiths, I.R., and Nave, K.A. (2003). Disruption of Cnp1 uncouples oligodendroglial functions in axonal support and myelination. Nat. Genet. *33*, 366–374.

Li, Y., Hibbs, M.A., Gard, A.L., Shylo, N.A., and Yun, K. (2012). Genome-wide analysis of N1ICD/RBPJ targets in vivo reveals direct transcriptional regulation of Wnt, SHH, and hippo pathway effectors by Notch1. Stem Cells *30*, 741–752.

Marcus, J., Honigbaum, S., Shroff, S., Honke, K., Rosenbluth, J., and Dupree, J.L. (2006). Sulfatide is essential for the maintenance of CNS myelin and axon structure. Glia *53*, 372–381.

Mason, J.L., Langaman, C., Morell, P., Suzuki, K., and Matsushima, G.K. (2001). Episodic demyelination and subsequent remyelination within the murine central nervous system: changes in axonal calibre. Neuropathol. Appl. Neurobiol. *27*, 50–58.

Matsui, T., Kanai-Azuma, M., Hara, K., Matoba, S., Hiramatsu, R., Kawakami, H., Kurohmaru, M., Koopman, P., and Kanai, Y. (2006). Redundant roles of Sox17 and Sox18 in postnatal angiogenesis in mice. J. Cell Sci. *119*, 3513–3526.

McCarthy, K.D., and de Vellis, J. (1980). Preparation of separate astroglial and oligodendroglial cell cultures from rat cerebral tissue. J. Cell Biol. *85*, 890–902.

Ming, X., Chew, L.J., and Gallo, V. (2013). Transgenic overexpression of Sox17 promotes oligodendrocyte development and attenuates demyelination. J. Neurosci. *33*, 12528–12542.

Moll, N.M., Hong, E., Fauveau, M., Naruse, M., Kerninon, C., Tepavcevic, V., Klopstein, A., Seilhean, D., Chew, L.J., Gallo, V., and Nait Oumesmar, B. (2013). SOX17 is expressed in regenerating oligodendrocytes in experimental models of demyelination and in multiple sclerosis. Glia *61*, 1659–1672.

Nait-Oumesmar, B., Decker, L., Lachapelle, F., Avellana-Adalid, V., Bachelin, C., and Baron-Van Evercooren, A. (1999). Progenitor cells of the adult mouse subventricular zone proliferate, migrate and differentiate into oligodendrocytes after demyelination. Eur. J. Neurosci. *11*, 4357–4366.

Scafidi, J., Hammond, T.R., Scafidi, S., Ritter, J., Jablonska, B., Roncal, M., Szigeti-Buck, K., Coman, D., Huang, Y., McCarter, R.J., Jr., et al. (2014). Intranasal epidermal growth factor treatment rescues neonatal brain injury. Nature *506*, 230–234.

Sohn, J., Natale, J., Chew, L.J., Belachew, S., Cheng, Y., Aguirre, A., Lytle, J., Nait-Oumesmar, B., Kerninon, C., Kanai-Azuma, M., et al. (2006). Identification of Sox17 as a transcription factor that regulates oligodendrocyte development. J. Neurosci. *26*, 9722–9735.

Stasiulewicz, M., Gray, S.D., Mastromina, I., Silva, J.C., Björklund, M., Seymour, P.A., Booth, D., Thompson, C., Green, R.J., Hall, E.A., et al. (2015). A conserved role for Notch signaling in priming the cellular response to Shh through ciliary localisation of the key Shh transducer Smo. Development *142*, 2291–2303.

Stolt, C.C., and Wegner, M. (2010). SoxE function in vertebrate nervous system development. Int. J. Biochem. Cell Biol. *42*, 437–440.

Stolt, C.C., Rehberg, S., Ader, M., Lommes, P., Riethmacher, D., Schachner, M., Bartsch, U., and Wegner, M. (2002). Terminal differentiation of myelin-forming oligodendrocytes depends on the transcription factor Sox10. Genes Dev. *16*, 165–170.

Stolt, C.C., Lommes, P., Sock, E., Chaboissier, M.C., Schedl, A., and Wegner, M. (2003). The Sox9 transcription factor determines glial fate choice in the developing spinal cord. Genes Dev. *17*, 1677–1689.

Wat, J.J., and Wat, M.J. (2014). Sox7 in vascular development: review, insights and potential mechanisms. Int. J. Dev. Biol. *58*, 1–8.

Watanabe, M., Toyama, Y., and Nishiyama, A. (2002). Differentiation of proliferated NG2-positive glial progenitor cells in a remyelinating lesion. J. Neurosci. Res. *69*, 826–836.

Woodruff, R.H., and Franklin, R.J.M. (1999). Demyelination and remyelination of the caudal cerebellar peduncle of adult rats following stereotaxic injections of lysolecithin, ethidium bromide, and complement/anti-galactocerebroside: a comparative study. Glia *25*, 216–228.

Yabut, O., Pleasure, S.J., and Yoon, K. (2015). A Notch above Sonic Hedgehog. Dev. Cell *33*, 371–372.

Yang, H., Lee, S., Lee, S., Kim, K., Yang, Y., Kim, J.H., Adams, R.H., Wells, J.M., Morrison, S.J., Koh, G.Y., and Kim, I. (2013). Sox17 promotes tumor angiogenesis and destabilizes tumor vessels in mice. J. Clin. Invest. *123*, 418–431.

Yuan, X., Chittajallu, R., Belachew, S., Anderson, S., McBain, C.J., and Gallo, V. (2002). Expression of the green fluorescent protein in the oligodendrocyte lineage: a transgenic mouse for developmental and physiological studies. J. Neurosci. Res. *70*, 529–545.

Zhang, Y., Argaw, A.T., Gurfein, B.T., Zameer, A., Snyder, B.J., Ge, C., Lu, Q.R., Rowitch, D.H., Raine, C.S., Brosnan, C.F., and John, G.R. (2009). Notch1 signaling plays a role in regulating precursor differentiation during CNS remyelination. Proc. Natl. Acad. Sci. USA *106*, 19162–19167.

Zhang, S., Zhu, X., Gui, X., Croteau, C., Song, L., Xu, J., Wang, A., Bannerman, P., and Guo, F. (2018). Sox2 is essential for Oligodendroglial proliferation and differentiation during postnatal brain myelination and CNS remyelination. J. Neurosci. *38*, 1802–1820.

Zhao, C., Ma, D., Zawadzka, M., Fancy, S.P.J., Elis-Williams, L., Bouvier, G., Stockley, J.H., de Castro, G.M., Wang, B., Jacobs, S., et al. (2015). Sox2 sustains recruitment of oligodendrocyte progenitor cells following CNS demyelination and primes them for differentiation during remyelination. J. Neurosci. *35*, 11482–11499.

Zhao, C., Deng, Y., Liu, L., Yu, K., Zhang, L., Wang, H., He, X., Wang, J., Lu, C., Wu, L.N., et al. (2016). Dual regulatory switch through interactions of Tcf7l2/Tcf4 with stage-specific partners propels oligodendroglial maturation. Nat. Commun. *7*, 10883.

STAR★METHODS

KEY RESOURCES TABLE

REAGENT or RESOURCE	SOURCE	IDENTIFIER
Antibodies		
Rabbit polyclonal NG2	MilliporeSigma	Cat#AB5320; RRID:AB_91789
Rabbit polyclonal Olig2	EMDMillipore	Cat# AB9610; RRID:AB_570666
Mouse monoclonal CC1	Calbiochem	Cat # OP-80; RRID:AB_2057371
Rabbit polyclonal MAG (H-300)	Santa Cruz Biotechnology	Cat # Sc-15324; RRID:AB_670104
Rabbit cleaved caspase 3	Cell Signaling Technologies	Cat #9661; RRID:AB_2341188
Rabbit Ki67	Abcam	Cat # Ab15580; RRID:AB_443209
Rat BrdU	Abcam	Cat# Ab6326; RRID:AB_305426
Rabbit TCF7L2	Abcam	Cat # Ab76151; RRID:AB_1310728
Goat TCF7L2	Santa Cruz Biotechnology	Cat # sc-8631; RRID:AB_2199826
Rabbit Sox2	Abcam	Cat# Ab97959; RRID:AB_306863
Rabbit Hes1	Abcam	Cat# Ab71559; RRID:AB_1209570
Rabbit Hes5	EMDMillipore	Cat# Ab5708; RRID:AB_91988
Rabbit Activated Notch1	Abcam	Cat# Ab8925; RRID:AB_306863
Rabbit Activated Notch1(Cl Val1744)	Cell Signaling Technologies	Cat #4147; RRID:AB_2153348
Chicken GFP/YFP	Aves	Cat # GFP-1020; RRID:AB_10000240
Mouse monoclonal MBP	Biolegend	Cat# 808402; RRID:AB_2564742
Mouse monoclonal CNPase	Biolegend	Cat# 836404; RRID:AB_2566639
Mouse monoclonal Actin	EMDMillipore	Cat# MAB1501R; RRID:AB_2223041
Rabbit polyclonal Sox17	ThermoFisher	Cat# PA5-72815; RRID:AB_2718669
Rabbit polyclonal Sox17	Abcam	Cat# Ab224637; RRID:AB_2801385
Alexa Fluor 647-Donkey Anti-Mouse IgG (H+L)	Jackson Immunoresearch Labs	Cat# 715-605-151; RRID: AB_2340863
Alexa Fluor 647-Donkey Anti-Rat IgG (H+L)	Jackson Immunoresearch Labs	Cat# 712-605-150; RRID:AB_2340693
Alexa Fluor 647-Donkey Anti-Chicken IgG (H+L)	Jackson Immunoresearch Labs	Cat# 703-605-155; RRID:AB_2340379
Alexa Fluor 594-Donkey Anti-Rabbit IgG (H+L)	Jackson Immunoresearch Labs	Cat# 711-585-152; RRID: AB_2340621
Alexa Fluor 594-Donkey Anti-Mouse IgG (H+L)	Jackson Immunoresearch Labs	Cat# 715-585-151; RRID: AB_2340855
Alexa Fluor 594 F(ab')$_2$ fragment Donkey Anti-Goat IgG (H+L)	Jackson Immunoresearch Labs	Cat #705-586-147; RRID: AB_2340434
Alexa Fluor 594- F(ab')$_2$ fragment Donkey Anti-Rat IgG(H+L)	Jackson Immunoresearch Labs	Cat# 711-586-153; RRID: AB_2340434
Alexa Fluor 488-Donkey Anti-Rabbit IgG (H+L)	Jackson Immunoresearch Labs	Cat# 711-545-152; RRID:AB_2340621
Alexa Fluor 488-Donkey Anti-Mouse IgG (H+L)	Jackson Immunoresearch Labs	Cat# 715-545-151; RRID:AB_2341099
Alexa Fluor 488-Donkey Anti-Mouse IgM, u chain specific	Jackson Immunoresearch Labs	Cat# 715-545-020; RRID:AB_2340844
Alexa Fluor 488-Donkey Anti-Rat IgG (H+L)	Jackson Immunoresearch Labs	Cat# 712-545-150; RRID:AB_2340683
Alexa Fluor 488-Donkey Anti-Goat IgG (H+L)	Jackson Immunoresearch Labs	Cat# 705-545-147; RRID:AB_2336933
Alexa Fluor 488-Donkey Anti-Chicken IgG (H+L)	Jackson Immunoresearch Labs	Cat# 703-545-155; RRID:AB_2340375
Goat anti-rabbit IgG-HRP	Cell Signaling Technology	Cat# 7074; RRID:AB_2099233
Goat anti-mouse IgG-HRP	Cell Signaling Technology	Cat# 7076; RRID:AB_330924
Chemicals, Peptides, and Recombinant Proteins		
PDGF-AB, recombinant human	MilliporeSigma	Cat# GF106
N2 supplement	Life Technologies	Cat# 17502048
D-Biotin	Sigma Aldrich	Cat# B4639
5-Bromo-2′-deoxyuridine (BrdU)	Sigma Aldrich	Cat# 203806 CAS number 59-14-3

(*Continued on next page*)

Continued

REAGENT or RESOURCE	SOURCE	IDENTIFIER
4',6'-diamidino-2-phenylindole (DAPI)	Sigma Aldrich	Cat# D9542 CAS:28718-90-3
Fluoromount-G	Fisher Scientific	Cat# OB100-01
DMEM high glucose	Life Technologies	Cat# 11995065
Hank's Balanced Salt Solution	Life Technologies	Cat# 14170112
OPTIMEM Reduced serum medium	Life Technologies	Cat# 31985070
Penicillin-Streptomycin 100X	Life Technologies	Cat# 15070063
Fetal Bovine Serum, Premium	Atlanta Biologicals	Cat# S11150
Lipofectamine 2000	Life Technologies	Cat# 11668-030
Poly L Lysine 30000-70000 MW	Sigma Aldrich	Cat# P9155 CAS:25988-63-0
Poly L ornithine 30000-70000 MW	Sigma Aldrich	Cat# P3655 CAS:27378-49-0
Paraformaldehyde	Sigma Aldrich	Cat# P6148 CAS:30525-89-4
Methanol	BDH	Cat# BDH1135-4LP CAS: 67-56-1
Ethanol	KOPTEC	Cat# DSP-MD-43 CAS: 6417-5
Hydrochloric Acid	Fisher Scientific	Cat# A144SI-212 CAS:7646-01-0
RIPA Buffer	Thermo Scientific	Cat# 89900
Halt Protease Inhibitor Cocktail	Thermo Scientific	Cat# 87786
DAPT N-[(3,5-Difluorophenyl)acetyl]-L-alanyl-2-phenyl]glycine-1,1-dimethylethyl ester	Millipore Sigma	Cat# 565770 CAS# 208255-80-5
Tamoxifen	Sigma Aldrich	Cat# T5648
Sunflower seed oil	Sigma Aldrich	Cat# 47123
L-α-lyso-lecithin	CalBiochem	Cat# 440154-100MG
Ketamine	Henry SCHEIN	ANADA 200-055 NDC 11695-6835-1
Xylazine	AKORN	NADA 139-236 NDC 59399-110-20
Bovin Serum Albumin	Sigma Aldrich	Cat# A7906 CAS:9048-46-8
Donkey Serum	Jackson Immunoresearch Lab	Cat# 017-000-121
Laemmli Sample buffer	Bio-Rad	Cat# 161-0737
10X TAE	K-D Medical	Cat# RGF-3310
10X PBS	K-D Medical	Cat# RGF-3210
10X Tris/Glycine/SDS buffer	K-D Medical	Cat# RGF-3390
10X Transfer Buffer	K-D Medical	Cat# RGF-3395
20X TBS	K-D Medical	Cat# RGF-3346
10X TBE	K-D Medical	Cat# RGE-3330
20X SSC	K-D Medical	Cat# RGF-3240
Triton X-100	Sigma Aldrich	Cat# T8787 CAS:9002-93-1
Tween-20	Sigma Aldrich	Cat# P9416 CAS:9005-64-5
Critical Commercial Assays		
In situ Cell Death detection kit, TMR red	Sigma Aldrich	Cat# 12156792910
Pierce BCA Protein Assay kit	ThermoFisher	Cat# 23227
Lightning Plus ECL	Perkin Elmer	Cat# NEL 103001EA
Supersignal West Dura Extended Duration ECL substrate	Thermo Fisher	Cat# 34075
RNeasy ® Micro kit	QIAGEN	Cat# 74004
iScript™ first strand cDNA synthesis kit	BioRad	Cat# 1708890
SYBR green qPCR mix with ROX	GeneCopoiea	Cat# QP031
NE-PER Nuclear and Cytoplasmic Extraction Reagents	ThermoFisher	Cat# 78833
LightShift™ Chemiluminescent EMSA kit	ThermoFisher	Cat# 20148
RNAScope – ms Sox17 probe	Advanced Cell Diagnostics	Cat# 493151-C2

(*Continued on next page*)

Continued

REAGENT or RESOURCE	SOURCE	IDENTIFIER
RNAScope – ms Olig2 probe-C1	Advanced Cell Diagnostics	Cat# 447091
RNAScope- ms PDGFRa probe-C1	Advanced Cell Diagnostics	Cat# 480661
RNAScope- EYFP-C3	Advanced Cell Diagnostics	Cat# 312131-C3
RNAScope pretreatment reagents	Advanced Cell Diagnostics	Cat# 322380
RNAScope Wash buffer	Advanced Cell Diagnostics	Cat# 310091
RNAScope Multiplex Fluorescent Reagent kit V2	Advanced Cell Diagnostics	Cat# 323100
TSA Plus Cyanine3/Cyanine5 System	Perkin Elmer	Cat# NEL 752001KT
Experimental Models: Organisms/Strains		
CNP-Cre knock-in mouse strain	Klaus Nave lab, Max Planck Inst	(Lappe-Siefke et al., 2003)
Sox17 floxed allele mouse strain	This study	N/A
R26R-EYFP mouse strain	Jackson Labs	Cat# 006148
PDGFRaCreERT2 mouse strain	Jackson Labs	Cat# 018280
CNPSox17ZsGreen transgenic mouse strain	Gallo lab, Children's National	(Ming et al., 2013)
Rat CRL SAS Sprague Dawley Timed pregnant E18	Charles River	Cat#400
Oligonucleotides		
See Table S1	NA	NA
Software and Algorithms		
LAS X Leica confocal software	Leica Microsystems	https://softadvice.informer.com/Leica_Confocal_Software.html
Olympus BX63 camera CellSens Standard 1.16 imaging software	Olympus Life Science	https://www.olympus-lifescience.com/en/software/cellsens/
SigmaPlot 13	Systat software, Inc	https://systatsoftware.com/products/sigmaplot/
Fiji ImageJ	ImageJ public freeware	https://imagej.net/Fiji/Downloads
Adobe Photoshop CC	Adobe Inc. Systems	https://www.adobe.com/creativecloud
Adobe Illustrator CC	Adobe Inc. Systems	https://www.adobe.com/creativecloud
Other		
Ms Sox17 Silencer Pre-designed siRNA	Ambion	Cat #AM16708A ID#69339,101960,101869
Rat Notch1 Select Pre-designed siRNA	Ambion	Cat #4390771 ID#s135114
4–20% polyacrylamide tris glycine SDS gel	BioRad	Cat#4561095

LEAD CONTACT AND MATERIALS AVAILABILITY

The mouse strain containing the Sox17 floxed allele was generated in this study. As this has not been deposited with an external centralized repository for its distribution, the Sox17 floxed allele generated in this study is available for sharing from the Lead Contact with a completed Materials Transfer Agreement. The CNPSox17 mouse line is available for sharing from the Lead Contact with a completed Materials Transfer Agreement. Other resources and reagents are available without restriction from the Lead Contact, Vittorio Gallo (VGallo@childrensnational.org).

EXPERIMENTAL MODEL AND SUBJECT DETAILS

Generation of Sox17 conditional knockout animals

A targeting construct containing all 5 exons of the mouse Sox17 gene was generated by Ingenious Targeting Laboratory (Stony Brook, NY). In this construct, exons 4 and 5, which encode the entire Sox17 coding region, are flanked by loxP sites, and the pGK-gb2 loxP/FRT Neo cassette lies 3′ to exon 5. The construct was linearized and electroporated into ES cells, and positive clones were isolated. Resultant chimeric mice with the targeted *Sox17^{flox}* conditional allele were bred with C57BL/6J mice (Stock 000664, Jackson Laboratory) to obtain heterozygous *Sox17^{flox}* offspring. The Neo cassette, which is flanked by two FRT sites, was excised by breeding with transgenic ''flipper'' mice ubiquitously expressing FLP recombinase. These mice were crossed with C57BL/6J mice, resulting in Neomycin-deleted *Sox17^{flox}*animals. Conditional *Sox17* mutants were subsequently generated by crossing female *Sox17$^{flox/flox}$* mice with male *CNP-cre$^{cre/+}$*; *Sox17$^{flox/flox}$* mice. The *CNP-Cre* knock-in mouse strain (Lappe-Siefke et al., 2003) is a kind gift from Dr Klaus-Armin Nave (Gottingen, Germany). The R26R-EYFP strain was purchased from the Jackson Laboratory (B6.129X1-*Gt(ROSA)26Sor$^{tm1(EYFP)Cos}$*/J, Stock 006148). The sequences of genotyping primers used to identify the floxed *Sox17*

allele, and CNP-Cre mice are as follows: *lox1 F*- CAG CCT TCC TAT TTC CCC AAG AGG; *lox3 R*- CTG GTC GTC ACT GGC GTA TCC; *cre F*- GCG GTC TGG CAG TAA AAA CTA TC; *cre R* - GTG AAA CAG CAT TGC TGT CAC TT. The deleted gene is identified with a 1000 bp product using *lox1*- CAG CCT TCC TAT TTC CCC AAG AGG; *KO R* CTA GTG TCA GGG ACT AGG AGG GAG (arrows Figures 1A and S1A). Although female CKO mice are sterile, the mutant mice are viable albeit producing small litters, with an apparently normal development and lifespan. OPC-specific Sox17 ablated mice were generated by breeding $Sox17^{flox}$ with *PDGFRa*creER^{T2} (018280, Jackson laboratory). Primers used genotyping are listed in Table S1. Tamoxifen (Sigma, 90 mg/ml) was dissolved in 100% ethanol and then diluted in autoclaved sunflower oil (Sigma) to a final concentration of 10 mg/ml. $Sox17^{flox/flox}$; *PDGFRa*creER$^{T2/+}$ were injected with 1 mg (neonates) or 75 mg/kg (P60) Tam once per day from −3 to −1 DPL. Control mice received 10% ethanol in sunflower oil. Due to the low frequency of mutant generation, results from male and female mutant mice are combined and averaged.

Mouse studies, Lysolecithin (LPC) demyelination and DAPT injections

All mouse experiments were performed according to protocols approved by the Institutional Animal Care and Use Committee at Children's National Hospital, Children's National Research Institute (Protocols 00030331, 00030337). Male and female mice were not analyzed as separate groups for the following reasons: neonates were not sexed, and genetic mutants are produced at very low frequency e.g., 1 in 10, and no more than 3 litters per breeder pair. For focal demyelination, adult mice were deeply anaesthetized using 100 mg/kg Ketamine and 10mg/kg Xylazine. Lysolecithin (1% L-α-lysophosphatidylcholine, 2μL, EMD chemicals) was injected unilaterally into the external capsule of 9-10 week old mice using a Hamilton syringe. On the contralateral side, 2μL of 0.9% NaCl was injected for control purposes. Injections were made using a stereotaxic apparatus at the following coordinates: 1.0 mm anterior to Bregma, 1.5 mm lateral, 2.0 mm deep. The date of injection was denoted as 0 days post lesion (DPL). Mice were allowed to recover for 7, 10, or 14 DPL and then perfusion-fixed with 4% paraformaldehyde for immunohistochemical analysis. *DAPT (gamma secretase inhibitor* N-[(3,5-Difluorophenyl)acetyl]-L-alanyl-2-phenyl]glycine-1,1-dimethylethyl ester. Tocris Bioscience, UK) was prepared in a final concentration of 50 uM in 2% DMSO in saline and injected using the same stereotaxic coordinates for cingulate WM as for LPC. Perfusion fixation was performed at 7 days post injection.

OL Progenitor cell culture, loss-of-function and DAPT studies

Purified rat cortical OPC cultures were prepared as previously described from embryonic day 20 SAS Sprague Dawley rats (Charles River Laboratories, Wilmington, MA), using a modified protocol for mixed glia culture (Ghiani et al., 1999a, 1999b; McCarthy and de Vellis, 1980). The E20 embryos isolated from uteri of timed pregnant dams are not sexed, and all embryonic cortical hemisphere tissue was combined. OPCs were isolated by differential plating following overnight shaking of flasks of mixed glia. OPCs were plated at a density of 500,000 cells per dish on poly-ornithine-coated 60 mm plastic Petri dishes or at 125,000 per well on poly-ornithine-coated, acid-cleaned 18 mm glass coverslips, and maintained in Dulbecco's modified Eagle's DME–N1 supplemented with 10 ng/ml platelet-derived growth factor (PDGF) (human AB, heterodimer form; Upstate Biotechnology, Lake Placid, NY) in biotin-containing DME-N1. Double-stranded Sox17 small interfering RNAs (siRNA) were purchased from Applied Biosystems. A combination of three Sox17 siRNAs containing ID101960, ID 69339 and ID 101869 was used (Sohn et al., 2006). OPCs were plated at 5×10^5 cells per 60 mm dish and treated with PDGF for 36 hr, then transfected in antibiotic-free DME-N1 with a 1:1:1 mixture of Sox17 siRNAs at a final concentration of 45 nM. using Lipofectamine 2000 (Invitrogen) at a siRNA:lipofectamine ratio of 20pmol:1ul for 24 or 48 h. Controls were mock-transfected with Lipofectamine reagent. Cells were allowed to recover for 48h before analysis by qPCR. Notch1 siRNA (ID s129953) was treated similarly. DAPT was added to PDGF-containing DME-N1 with biotin 6-24h after plating at the indicated final concentrations. 5-Bromo-2′-deoxyuridine (BrdU, MilliporeSigma) was added to a final concentration of 50 uM 12 h before fixation with 4% paraformaldehyde and analysis by immunocytochemistry for Sox2 and BrdU.

METHOD DETAILS

Immunohistochemistry and TUNEL assay

Mice were anesthetized with isoflurane and perfused with 0.1M PBS, pH 7.4, followed by 4% paraformaldehyde (PFA). The brains were removed and fixed in 4% PFA overnight at 4°C. 45 μm coronal sections cut using a vibratome (Leica) or freezing microtome (Leica) following cryoprotection in 20% and 10% glycerol. Immunohistochemistry was performed on floating sections using methods previously described in Yuan et al., 2002. The following antibodies were used: rabbit anti-NG2 (1:500,Millipore), rabbit anti-Olig2 (1:500; Millipore), mouse anti-CC1 (1:1000; Calbiochem), rabbit MAG (1:300, Santa Cruz Biotechnology), rabbit anti-caspase3 (1:250; Cell Signaling), rabbit anti-ki67 (1:200; Abcam), rat anti-BrdU (1:250; Abcam), goat anti-TCF7L2 (1:150, Santa Cruz Biotechnology), rabbit anti-TCF7L2 (1:500, Abcam), Rabbit anti-Sox2 (1:500, Abcam), rabbit anti-Hes1 and Hes5 (1:300, Millipore), rabbit anti-Activated Notch1 (1:400, Abcam), and chicken anti-GFP/YFP (1:1000, Aves labs, Inc). Corresponding secondary antibodies were used at a 1:600 dilution (Jackson Immunoresearch Laboratories). Sections were mounted on slides and covered in Fluoromount G + DAPI (Southern Biotechnology). TUNEL assays were performed with tissue sections using the *In Situ* Cell Death detection kit, TMR red (Roche Life Science) according to manufacturer's instructions. TUNEL procedures preceded immunohistochemistry for CC1 and MAG.

Confocal Microscopy and image acquisition

Stained tissue sections were imaged on either a Zeiss LSM 510, Olympus FV1000 or Leica TCS SP8 laser scanning confocal microscope, acquired with Zen or LasX under 40X or 63X oil objective respectively, using a Z step of 0.75 um. Demyelinated lesions were confirmed by a decrease or absence of CC1 and MBP immunoreactivity, and disruption of WM cytoarchitecture. For saline-injected tissue, the injection site was located based on identification of the needle track, and injection site on the skull surface.

Western Blot analyses

Coronal brain sections 200 um thick were made on a McIlwain tissue chopper and placed in ice-cold DMEM. The corpus callosum was carefully micro-dissected from tissues between bregma 1.32mm and −2.12mm and homogenized in RIPA-lysis buffer (Santa Cruz Biotechnology, Inc). Cultured oligodendrocyte progenitor cells in dishes were harvested gently by rubber cell scraper into cold PBS containing Halt protease inhibitors(ThermoFisher) and pelleted by centrifugation. Total protein extracts and western blot analysis were prepared as previous described (Chew et al., 2011). Briefly, tissue was extracted by homogenization in RIPA buffer containing Halt protease inhibitors (ThermoFisher), cleared by centrifugation at 13,000 rpm at 4C and the supernatant analyzed for protein concentration. 15-30 ug protein per well was resolved on 4%–20% Tris-Glycine-SDS polyacrylamide gels (Biorad) and transferred onto PVDF membranes. After transfer, the membranes were blocked in either 4% milk or 5% BSA for 1 hr at room temperature, and then incubated overnight with primary antibodies diluted in either 4% milk or 5% BSA. The following primary antibodies were used: mouse anti-MBP (1:1000, Covance), anti-actin (1:5000, Chemicon), mouse anti-CNP (1:500; Covance), rabbit anti-MAG (1:500; Santa Cruz), rabbit anti-Sox2 and TCF7L2 (1:1000; Abcam). Activated Notch1 (Cell Signaling) was used at 1:1200. After washing with TBS-containing Tween20 (0.1%v/v), membranes were incubated with HRP-conjugated secondary antibodies (Cell Signaling Technology) diluted at a concentration of 1:5000 in blocking buffer for 1hr at room temperature. After washing, signals were developed using either Lightning Plus ECL (Perkin Elmer) or Supersignal West Dura Extended Duration ECL substrates (Thermo Fisher).

Quantitative PCR

The corpus callosum was micro-dissected as described above and RNA was extracted with RNeasy Micro Kit (QIAGEN). Primary OPCs were collected in 350ul RLT buffer per 60mm dish and extracted in a manner similar to tissue. Total RNA (0.5-1 ug) was used to synthesize cDNA using SuperScript III First strand synthesis system (Life Technologies) or iScript synthesis kit (BioRad) in a 20ul reaction. Primer sequences are provided in Table S1. qPCR was carried out using diluted cDNA with SYBR Green qPCR mix (Sigma-Aldrich or GeneCopoiea) in 20-25 ul reactions a 96 well spectrofluorometric thermal cycler (ABI Prism 7900 HT Sequence Detector System; Applied Biosystems). Cycling conditions were as follows: Stage 1 95°C 10 min, Stage 2 40 cycles 95°C 45 s, 56-60°C 45 s, 72°C 45 s. Baseline values lie between cycles 8 and 15. Mean fold gene expression normalized against beta-actin was calculated with ABI software with the 2 (Delta Delta CT) Method. Data are expressed as mean fold change ± SEM with respect to reference control group.

Behavioral analysis

Mice were tested on the inclined, elevated beam-walking task at ages P30 and P60 as previously described (Brooks and Dunnett, 2009; Carter et al., 2001; Scafidi et al., 2014). Briefly, a 80 cm long wooden beam of 2cm or 1cm width was placed at a 30-degree angle, raised about 45 cm from the bench surface. A dark box with bedding was positioned at the top of the incline and served as the destination. Mice were placed at the lower end of the 2cm beam, and trained to walk across it into the dark box. After training, the width of the beam was reduced to 1cm to assess motor coordination. Four consecutive trials were recorded, and between each trial the animal was returned to its home cage for at least 15 min. A blinded experimenter observing from above, assessed mouse performance by documenting the number of foot slips (either hind legs or front legs) and the time to traverse the beam.

Electron Microscopy

Mice were prepared for electron microscopic analysis as previously described (Aguirre et al., 2007; Marcus et al., 2006). Following transcardial perfusion with 0.1M Millonig's buffer containing 4% paraformaldehyde and 2.5% glutaraldehyde and brain removal, a coronal brain matrix (Ted Pella, Redding, CA) was used to cut the brain in serial 1 mm slices. Comparable slices for each brain (~0.5mm anterior to bregma were rinsed 3X in 0.1M cacodylate buffer, post fixed in 1% osmium tetroxide (in cacodylate buffer), dehydrated in increasing dilutions of ethanol and embedded in PolyBed resin. Thick (1μm) and thin (70nm) sections were stained with toluidine blue or with a combination of uranyl acetate and lead citrate, respectively. A minimum of 10 electron micrographs within the corpus callosum region were captured at both low (5,000X) and high (20,000X) magnifications per mouse using a JEOL JEM 1230 transmission electron microscope equipped with a Gatan 4K X 4K Ultrascan digital camera.

Electrophoretic Mobility Shift Assays

Nuclear lysates from P12 white matter tissue and OPC cells cultured for 2 days in 10 ng/ml PDGF were prepared by using the Thermo Scientific NE-PER nuclear and cytoplasmic extraction reagents according to the manufacturer's instructions. The SoxA(SxA) probe was derived from hmSox-a, (Chiang et al., 2017) and SoxB(SxB) probe was derived from hmSox-b, (Chiang et al., 2017; Table S1). Double-stranded probes were labeled with biotin on both ends of one strand (IDTDNA, Coralville, IA). Binding assays were performed

using the LightShift™ Chemiluminescent EMSA kit according to manufacturer's directions. Briefly, approximately 7-10 ug of nuclear protein was incubated with 20 fmol of biotinylated probe in 20ul reactions containing 1x Binding buffer, 2.5% glycerol, 50 ng/ml poly (dI.dC) and 5 mM $MgCl_2$. 4 pmol unlabeled oligonucleotides (EBNA Control 5′-TAGCATATGCTA-3′ from LightShift™ kit, or SoxA(SxA) or SoxB(SxB)) were added in competition experiments, and 1-2ul of Sox17 antibody (Abcam ab224637 (Antibody S1; Figure 5)) or Thermo PA5 72815 (S2; Figure 5)) was added to the reactions 30 mins prior to loading the gel. After adding 5 ul of 5X loading buffer, the reactions were resolved on 5% nondenaturing polyacrylamide gels and subsequently transferred onto Biodyne™ Nylon membrane at 100V in 0.5X TBE. Blocking, incubation with Streptavidin-HRP, washing and visualization procedures were performed using reagents in the Chemiluminescent Nucleic Acid Detection Module (ThermoFisher Scientific). The membranes were exposed to X-ray film for 2-5 mins.

In situ hybridization

Following perfusion fixation with 4% paraformaldehyde, whole brain specimens were post-fixed in 4% paraformaldehyde for 24 h, then cryoprotected through 10%, 20% and 30% sucrose solutions in PBS, each for 24h at 4°C. After freezing in O.C.T., frozen coronal sections 14 um thick were used for *in situ* hybridization experiments with RNAscope reagents (Advanced Cell Diagnostics), and according to the vendor's protocols for fluorescent multiplex assays. Only minor modifications were taken during pretreatment procedure: Tissue sections were pretreated first with PBS, then 4% paraformaldehyde and progressively dehydrated through a 50, 70, 100% ethanol series of 2 mins each and bake-dried for 10 mins at 60°C before incubation with hydrogen peroxide from the ACD RNAscope Pretreatment kit. After rinsing with water twice and allowing the slides to dry, a hydrophobic barrier was traced around the sections and dried for 20 mins before proceeding with Protease III incubation for 30 min in the Hyb-EZ oven (ACD). After rinsing in water, probe hybridization was performed in a volume of 140 ul. The remainder of the procedure- probe hybridization, amplification and TSA fluorophore tagging (diluted to 1:1500) - were performed according to the ACD protocol for RNAscope Multiplex Fluorescent Reagent Kit v2 Assay, Document number 323100-USM without modification. Images were captured on the Leica TCS SP8 laser scanning confocal microscope with the 63X oil objective with Z step of 0.5 um. Higher resolution images were captured with the same objective using Zoom scaling of 1.5x.

QUANTIFICATION AND STATISTICAL ANALYSIS

Confocal image analysis

Images were analyzed using ImageJ software for the parameter outlined for each experiment. At least 3 sections per lesion were imaged per animal, at evenly spaced intervals (e.g., one in every 4 sections). The lesion area was imaged using tiling. For cell density calculations, the number of cells per parameter was divided by the total volume of the z stacked image (length x width x stacked depth) to give cells/um3. Measurements were then multiplied by 10^6 to give cells/10^6 um^3. Images of cingulate white matter and corpus callosum white matter up to the dorsal edge of, but not including, the subventricular zone, were taken at the same laser intensity and microscope acquisition settings for 3 sections per animal. ImageJ was used to image the WM area, form z stacks and adjust the threshold. Images were minimally adjusted for clarity and size using Adobe Photoshop software.

Electron microscope image analysis

Low-magnification images were used to qualitatively assess the overall extent of myelination; high-magnification images were used for quantitative analyses. The percent myelinated and unmyelinated axons was determined and G ratio analysis was conducted. Any axon with a single wrap of an oligodendrocyte process was classified as ''myelinated''; G ratio analyses were limited to only myelinated axons and were calculated by dividing the average axon diameter determined by measuring the longest and shortest diameter by the average axon diameter plus the width of the thickest and narrowest span of the myelin sheath in cross section. For myelin thickness measurements, regions with expanded myelin due to structural artifact were not used. Analyses were limited to axons with a caliber of >0.3 μm since previous work has shown that CNS axons $\leq$ 0.3μm are not myelinated (Mason et al., 2001).

Corpus Callosum thickness

Measurement of corpus callosum thickness in coronal sections was performed on images captured on the Olympus BX63 fluorescence microscope using the 10X objective and by using the line drawing tool of ImageJ. Six lines, three on either side of the midline, distributed evenly between the midline and cingulate white matter, were drawn perpendicular to opposite edges of the corpus callosum. Their lengths in um were recorded. At least 2 lines were drawn and their average recorded for each location. Two consecutive sections were measured per brain sample, and averages calculated for each location. 4 brain samples (n = 4) were analyzed per group.

In situ hybridization signal analysis

PDGFRa-expressing cells were identified based on the presence of dot clustering in its channel. Only PDGFRa cells with 10 or more dots were considered positive. Olig2-expressing cells were treated similarly, whereas YFP-C3 criterion was a minimum of 5 dots. These criteria were applied in the estimation of Cre recombination efficiency by YFP expression. For quantification of fluorescent RNA signal, the number of dots or grains per cell with visible DAPI-stained nucleus was estimated by manual counting in ImageJ.

The absolute number of Sox17-C2 dots was counted only in PDGFRa-positive cells. Sox17-C dots were counted in a total of about 60 PDGFRa cells in each group i.e., 2 higher magnification images from each of 3 brains. The average number of dots per PDGFRa-expressing cell was compared between groups.

Statistical analysis

All statistical analyses were performed with Sigmaplot 13, and all values are expressed as mean ± SEM, and illustrations were created using SigmaPlot 13. Neonatal mice sometimes died from early tamoxifen injections, so these samples could not be analyzed. The specific numbers of animals or cultures are denoted in each figure legend. Significance was determined using SigmaPlot13 software, with Student's unpaired, two-tailed t tests for comparisons between two groups and one-way ANOVA with Holm-Sidak post hoc tests for multiple comparisons. N values denote independent experiments. The degree of statistical significance was indicated with asterisks as defined in figure legends.

DATA AND CODE AVAILABILITY

This study did not generate any unique datasets or code.